38. Holt RR, Lazarus SA, Sullards MC, *et al.* Procyanidin dimer B2 [epicatechin-(4β-8)-epicatechin] in human plasma after the consumption of a flavanol-rich cocoa. *Am J Clin Nutr* 2002; **76**:798–804.

39. Zhu QY, Schramm DD, Gross HB, *et al.* Influence of cocoa flavanols and procyanidins on free radical-induced human erythrocyte hemolysis. *Clin Dev Immunol* 2005; **12**:27–34.

Accepted for publication 20 February 2010

Bioorganic & Medicinal Chemistry Letters 20 (2010) 354–358

Contents lists available at ScienceDirect

Bioorganic & Medicinal Chemistry Letters

journal homepage: www.elsevier.com/locate/bmcl

CD4 mimics targeting the mechanism of HIV entry

Yuko Yamada [a], Chihiro Ochiai [a], Kazuhisa Yoshimura [b], Tomohiro Tanaka [a], Nami Ohashi [a], Tetsuo Narumi [a], Wataru Nomura [a], Shigeyoshi Harada [b], Shuzo Matsushita [b], Hirokazu Tamamura [a,*]

[a] Institute of Biomaterials and Bioengineering, Tokyo Medical and Dental University, Chiyoda-ku, Tokyo 101-0062, Japan
[b] Center for AIDS Research, Kumamoto University, Kumamoto 860-0811, Japan

ARTICLE INFO

Article history:
Received 19 September 2009
Revised 20 October 2009
Accepted 22 October 2009
Available online 4 November 2009

Keywords:
CD4 mimic
HIV entry
Synergistic effect
CXCR4

ABSTRACT

A structure–activity relationship study was conducted of several CD4 mimicking small molecules which block the interaction between HIV-1 gp120 and CD4. These CD4 mimics induce a conformational change in gp120, exposing its co-receptor-binding site. This induces a highly synergistic interaction in the use in combination with a co-receptor CXCR4 antagonist and reveals a pronounced effect on the dynamic supramolecular mechanism of HIV-1 entry.

Recently, remarkable success has attended the clinical treatment of HIV-infected and AIDS patients, with 'highly active antiretroviral therapy (HAART)'. This approach involves a combination of two or three agents from two categories: reverse transcriptase inhibitors and protease inhibitors.[1] In addition, the molecular mechanism involved in HIV-entry and -fusion into host cells has been described in detail.[2] The complex interactions of surface proteins on cellular and viral membranes, which are designated as a dynamic supramolecular mechanism of HIV entry, are reported to be crucial to the viral infection. In a first step, an HIV envelope protein, gp120 interacts with a cell surface protein, CD4, leading to a conformational change in gp120 followed by subsequent binding of gp120 to a co-receptor CCR5[3] or CXCR4.[4] CCR5 and CXCR4 are the major co-receptors for the entry of macrophage-tropic (R5-) and T cell line-tropic (X4-) HIV-1, respectively. The interaction of gp120 with CCR5 or CXCR4 triggers entry of another envelope protein, gp41 to the cell membrane and formation of a gp41 trimer-of-hairpins structure, which causes fusion of HIV/cell-membranes and completes the infection.

Informed by this mechanism, a fusion inhibitor, enfuvirtide (fuzeon, Trimers & Roche)[5] and a CCR5 antagonist, maraviroc (Pfizer)[6] in addition to an integrase inhibitor, raltegravir (Merck)[7] have been used clinically. However, serious problems with chemotherapy still persist, including the emergence of viral strains with multi-drug resistance (MDR), considerable adverse effects and high costs. Consequently, development of novel drugs possessing mechanisms of action different from those of the above inhibitors is currently required. We have previously developed selective CXCR4 antagonists[8] and fusion inhibitors.[9] Furthermore, *N*-(4-Bromophenyl)-*N'*-(2,2,6,6-tetramethylpiperidin-4-yl)-oxalamide (**1**) and *N*-(4-chlorophenyl)-*N'*-(2,2,6,6-tetramethylpiperidin-4-yl)-oxalamide (**2**) were previously found using chemical library screening to inhibit syncytium formation by other researchers.[10] **1** and **2** bind to gp120 with binding affinities of K_d = 2.2 μM and 3.7 μM, respectively, blocking the interaction of gp120 with CD4 in the first step of an HIV-1 entry. Thus, in the present study we focus on the development of CD4 mimics that can block the interaction between gp120 and CD4. We have investigated the effect of CD4 mimics on conformational changes of gp120 and on their use in combination use with a CXCR4 antagonist.

Initially, molecular modeling of compound **2** docked into gp120 was carried out using docking simulations performed by the FlexSIS module of SYBYL 7.1 (Tripos, St. Louis) (Fig. 1).[11] The atomic coordinates of the crystal structure of gp120 with soluble CD4 (sCD4) were retrieved from Protein Data Bank (PDB) (entry 1RZJ) (Fig. 1a) and it was observed that Phe^{43} and Arg^{59} of the CD4 have multiple contacts with Asp^{368}, Glu^{370} and Trp^{427} of gp120, which are all conserved residues. An inspection of the environment of compound **2** docked in gp120 revealed the presence of a large cavity around the *p*-position of the phenyl ring of compound **2**, which could interact with the viral surface protein gp120 (Fig. 1b and c). Several analogs of **2** with substituents on the phenyl ring were therefore synthesized.

All compounds except **12** were synthesized by previously published methods (Scheme 1).[10b,12,13] Aniline derivatives (**3**) were coupled with ethyl oxalyl chloride to yield the corresponding ethyl oxalamates **4**. Saponification of the above oxalamates to the corresponding free acids and the subsequent coupling with 4-ami-

* Corresponding author.
E-mail address: tamamura.mr@tmd.ac.jp (H. Tamamura).

0960-894X/$ - see front matter © 2009 Elsevier Ltd. All rights reserved.
doi:10.1016/j.bmcl.2009.10.098

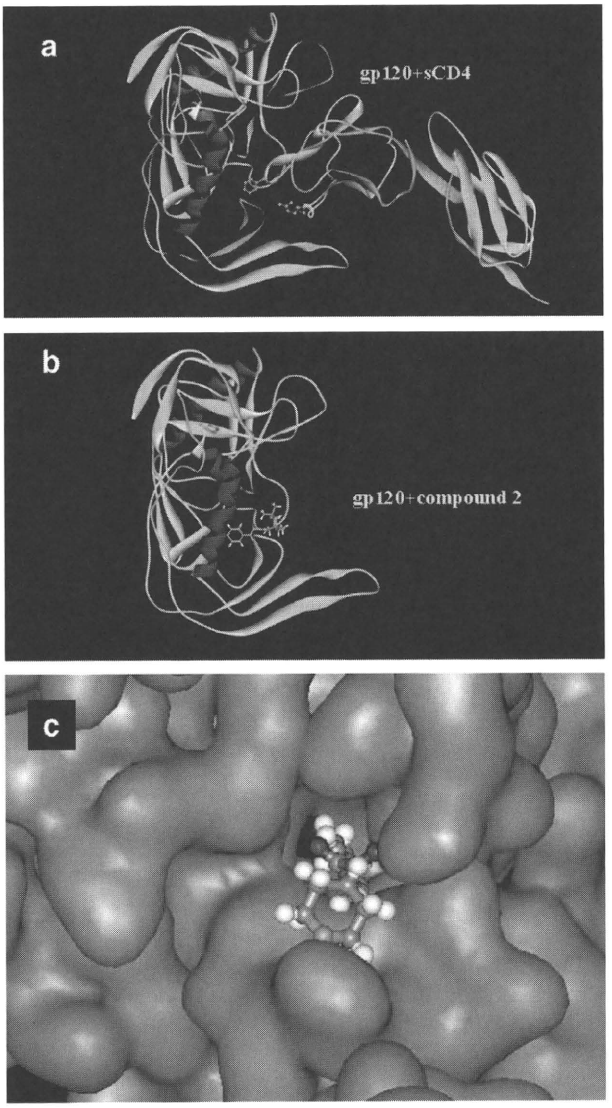

Figure 1. (a) The crystal structure of gp120 with soluble CD4 (sCD4) retrieved from the PDB (entry 1RZJ); (b) docking structure of compound **2** and gp120; (c) a focused figure of (b) shown by space-filling model.

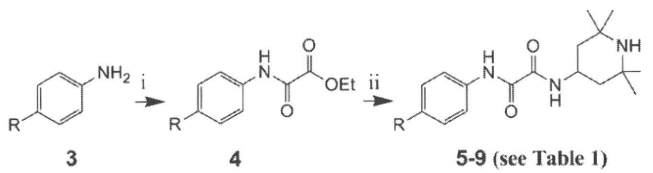

Scheme 1. Reagents and conditions: (i) ethyl oxalyl chloride, Et_3N; (ii) 1 M NaOH; 4-amino-2,2,6,6-tetramethylpiperidine, 1-(3-dimethylaminopropyl)-3-ethylcarbodiimide hydrochloride, 1-hydroxybenzotriazole, Et_3N.

no-2,2,6,6-tetramethylpiperidine using 1-ethyl-3-(3-dimethylaminopropyl)carbodiimide hydrochloride (EDC) and 1-hydroxybenzotriazole (HOBt) yielded compounds **5–9**. In the case of compound **12**, whose amide bond is not stable during the reaction of the saponification of the corresponding oxalamates, an alternative synthetic scheme was used (Scheme 2).[14] The reaction of *p*-nitroaniline (**10**) with oxalyl chloride gave the corresponding oxoacetamide **11**, which was subsequently coupled with 4-amino-2,2,6,6-tetramethylpiperidine to yield the desired compound **12**.

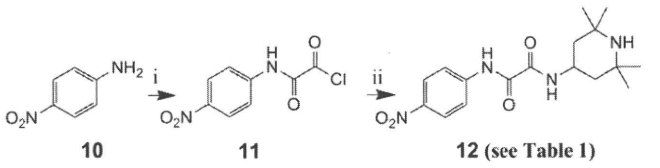

Scheme 2. Reagents and conditions: (i) oxalyl chloride, Et_3N; (ii) 4-amino-2,2,6,6-tetramethylpiperidine, Et_3N.

The anti-HIV activity of the synthetic compounds was evaluated against various viral strains including both laboratory and primary isolates (Table 1). IC_{50} values were determined by the 3-(4,5-dimethylthiazol-2-yl)-2,5-diphenyltetrazolium bromide (MTT) method[15] as the concentrations of the compounds which conferred 50% protection against HIV-1-induced cytopathogenicity in PM1/CCR5 cells. Cytotoxicity of the compounds based on the viability of mock-infected PM1/CCR5 cells was also evaluated using the MTT method. CC_{50} values were determined as the concentrations achieving 50% reduction of the viability of mock-infected cells. Compounds **1** and **2** showed potent anti-HIV activity against laboratory isolates, IIIB (X4, Sub B) and 89.6 (dual, Sub B) strains, and compound **2** also possessed potent activity against a primary isolate, an fTOI strain (R5, Sub B). All of the IC_{50} values were between 4 μM and 10 μM. Compound **1** was not tested against primary isolates. The potencies of compounds **1** and **2** are comparable to the reported binding affinities for gp120 (K_d = 2.2 and 3.7 μM, respectively).[10] Several of the new analogs of compounds **1** and **2** showed significant anti-HIV activity. Compound **5**, which has a phenyl group in place of the *p*-chlorophenyl group of compound **2**, did not show significant anti-HIV activity at concentrations below 100 μM against all strains tested except for an fTOI strain (R5, Sub B). This result suggests that a substituent at the *p*-position of the phenyl ring is critical for potent activity. Compound **6**, which has a fluorine atom at the *p*-position of the phenyl ring, showed moderate anti-HIV activity against laboratory isolates, IIIB (X4, Sub B) and 89.6 (dual, Sub B) strains (IC_{50} = 61 and 81 μM, respectively), but, at concentrations below 100 μM, failed to show significant anti-HIV activity against a primary isolate, a KYAG strain (R5, Sub B). Among halogen atoms, fluorine is less suitable than bromine or chlorine as a substituent at the *p*-position of the phenyl ring, as evidenced by compound **6**, which is 8–15-fold less potent than compounds **1** and **2** against IIIB (X4, Sub B) and 89.6 (dual, Sub B) strains. Compound **7**, which has a methyl group at the *p*-position of the phenyl ring, showed relatively more potent activity against IIIB (X4, Sub B) and 89.6 (dual, Sub B) strains (IC_{50} = 23 and 41 μM, respectively) than compound **6**. Compound **7** also showed significant anti-HIV activity against primary isolates, fTOI (R5, Sub B) and KYAG (R5, Sub B) strains (IC_{50} = 16 and 51 μM, respectively). Compound **8**, with a methoxy group at the *p*-position of the phenyl ring, did not show significant anti-HIV activity against all strains tested until a concentration of 100 μM was reached. In the biological assays, derivatives having electron-withdrawing substituents such as bromine, chlorine and fluorine at the *p*-position of the phenyl ring are relatively potent, whereas derivatives having electron-donating groups such as methoxy at this position are not potent. Furthermore, the steric effect of a substituent at the *p*-position of the phenyl ring appears to be critical to anti-HIV activity. The sum of Hammett constants (σ) of benzoic acid substituents[16] shown in Table 1 can be used to evaluate the electron-withdrawing or -donating effect of the substituents on the aromatic ring. The Taft E_s values[16a,17] were used as steric parameters for substituents at the *p*-position of the phenyl ring. The order of potency found for the halogen-containing derivatives in anti-HIV activity against laboratory isolates, IIIB (X4, Sub B) and 89.6 (dual, Sub B), is: compound **1** (R = Br) (σ = 0.23, E_s = −1.16), **2**

Table 1
Hammett constants (σ) and steric effects (E_s) of substituted aromatic rings and anti-HIV activity and cytotoxicity of synthetic compounds

Compd	R[a]	σ[b]	E_s[c]	IC_{50}[e] (μM)				CC_{50}[e] (μM)
				Lab. isolates		Primary isolates		
				IIIB (X4)	89.6 (dual)	fTOI (R5)	KYAG (R5)	
1	Br	0.23	−1.16	4	9	ND	ND	150
2	Cl	0.23	−0.97	8	10	5	>30	170
5	H	0	0	>100	>100	81	>100	350
6	F	0.06	−0.46	61	81	ND	>100	320
7	CH_3	−0.17	−1.24	23	41	16	51	210
8	OCH_3	−0.27	−0.55	>100	>100	ND	>100	340
9	CF_3	0.54	−2.40	ND	27	ND	ND	72
12	NO_2	0.78	−1.77[d]	ND	42	ND	ND	230
sCD4				0.010	0.021	0.0044	ND	ND

[a] See Schemes 1 and 2.
[b] σ = Hammett constant of a substitutent on a benzoic acid derivative.[16]
[c] E_s = steric effect of a substituent at the *para* position on the aromatic ring.[16a,17]
[d] The average value of −1.01 and −2.52, which are E_s values of the NO_2 group, −1.77, was used.
[e] Values are means of at least three experiments (ND = not determined).

(R = Cl) (σ = 0.23, E_s = −0.97), **6** (R = F) (σ = 0.06, E_s = −0.46) and **5** (R = H) (σ = 0, E_s = 0). This is the order of substituents' electron-withdrawing ability and also of their size. Methyl (σ = −0.17, E_s = −1.24) is an electron-donating group, but is almost as bulky as a bromine atom. Thus, the *p*-methyl derivative **7** has relatively potent anti-HIV activity against laboratory isolates, IIIB (X4, Sub B) and 89.6 (dual, Sub B), higher than that of compound **6** (R = F) but lower than that of compound **1** (R = Br) or **2** (R = Cl). The electron-donating ability of a methoxy group is stronger (σ = −0.27), but the bulk size is smaller (E_s = −0.55), than that of a methyl group. Thus, the *p*-methoxy derivative **8** has no significant anti-HIV activity against all strains tested at concentrations below 100 μM. Two derivatives containing bulkier and more potent electron-withdrawing substituents such as trifluoromethyl (R = CF_3) (σ = 0.54, E_s = −2.40) and nitro (R = NO_2) (σ = 0.78, E_s = −1.77) at the *p*-position of the phenyl ring were evaluated. Compounds **9** (R = CF_3) and **12** (R = NO_2) showed significant anti-HIV activity against an 89.6 (dual, Sub B) strain. These are less potent than compounds **1** and **2** and this is perhaps due to the excessive size of the substituents at the *p*-position. This suggests that a certain level of the bulk size and a potent electron-withdrawing ability of the substituents are preferable for anti-HIV activity. It is estimated that a cavity around the *p*-position of the phenyl ring of CD4 mimicking compounds would be optimally filled by bromine (E_s = −1.16) or a methyl group (E_s = −1.24) at *p*-position, and that an electron-deficient aromatic ring might interact tightly with a negatively charged group such as carboxy of Glu^{370}. In isothermal titration calorimetry (ITC) experiments reported elsewhere,[10c] compound **5** (R = H) does not have significant affinity for gp120, and compound **6** (R = F) has less potent affinity for gp120 than compound **2**, consistent with the present data. In all but one of the compounds, no significant cytotoxicity was detected (CC_{50} >150 μM, Table 1), the exception being compound **9** (R = CF_3) (CC_{50} = 72 μM). Compounds **7** and **12** have relatively low cytotoxicities, compared to compounds **1** and **2**.

Fluorescence activated cell sorting (FACS) analysis was performed[15] to investigate whether these synthetic compounds interact with gp120 inducing the conformational change necessary for the approach of an anti-envelope antibody or a co-receptor to the gp120. The profile of binding of an anti-envelope CD4-induced monoclonal antibody, 4C11, to the Env-expressing cell surface (an R5-HIV-1 strain, JR-FL,-infected PM1 cells) pretreated with the above CD4 mimic analogs was examined. Comparison of the binding of 4C11 to the cell surface was measured in terms of the mean fluorescence intensity (MFI), and is shown in Figure 2. Pretreatment of the Env-expressing cells with compound **2** (MFI = 38.42) produced a remarkable increase in binding affinity for 4C11, similar to that observed in pretreatment with sCD4 (MFI = 37.90). This is consistent with the results in the previous paper[10] where it was reported that compound **2** enhances the binding of gp120 to the 17b monoclonal antibody which recognizes the co-receptor binding site of gp120. Env-expressing cells, which were not pretreated with sCD4 or a CD4 mimic compound, did not show significant binding affinity for 4C11 (Fig. 2, blank). The increase in binding affinity for monoclonal antibodies may be due to conformational changes in gp120, which were caused by the interaction of sCD4 or a CD4 mimic with gp120. It is hypothesized that such conformational changes involve the exposure of the co-receptor binding site of gp120 (the V3 loop), which is hidden internally, since the binding of gp120 to 17b is enhanced. Compound **5**, which failed to show significant anti-HIV activity, and compounds **7**, **9** and **12**, which had significant anti-HIV activity, were assessed in the FACS analysis. The profile of the binding of 4C11 to the Env-expressing cell surface pretreated with compound **5** (MFI = 14.34) was similar to that of the blank (MFI = 11.24), suggesting that compound **5** offers no significant enhancement of binding affinity for 4C11. This result is compatible with the anti-HIV activity of compound **5**. The profile of the binding of 4C11 to the Env-expressing cell surface pretreated with compound **7** (MFI = 38.33) was entirely similar to that of compound **2** used as a pretreatment. Pretreatment of the cell surface with compounds **9** and **12** (MFI = 29.09 and 30.01, respectively) produced a slightly lower enhancement of binding affinity for 4C11, compared to those of compounds **2** and **7** as pretreatments. However, in the ITC experiments reported elsewhere,[10c] compound **9** (R = CF_3) has a high affinity for gp120, comparable to that of compound **2**, but compound **12** (R = NO_2) does not have significant affinity for gp120, indicating that these are not consistent with the current FACS studies, possibly due to the difference in the assay systems. Although the anti-HIV activity of **7** is weaker than that of compound **2**, the level of compound **7** inducing an enhancement of binding affinity of gp120 for 4C11 is comparable to that of compound **2**. The concentration of compounds used in the FACS analysis was 100 μM, much beyond the IC_{50} values of compounds **2** and **7**. A concentration of 100 μM would be also sufficient for the expression of anti-HIV activity caused by compounds **2** and **7**.

An effect on the use of compound **2** combined with another entry inhibitor was investigated. Analysis of the synergistic effects of anti-HIV agents was performed according to the median effect principle using the CalcuSyn version 2 computer program[18] to estimate IC_{50} values of compounds in different combinations. Combination indices (CI) were estimated from the data evaluated using the MTT assay

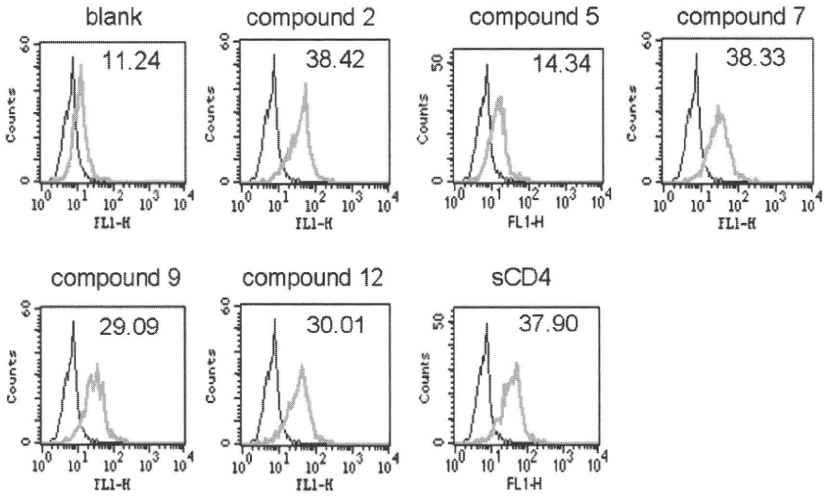

Figure 2. JR-FL (R5, Sub B) chronically infected PM1 cells were preincubated with 100 μM of a CD4 mimic or sCD4 (11 nM) for 15 min, and then incubated with an anti-HIV-1 mAb, 4C11, at 4 °C for 15 min. The cells were washed with PBS, and fluorescein isothiocyanate (FITC)-conjugated goat anti-human IgG antibody was used for antibody-staining. Flow cytometry data for the binding of 4C11 (green lines) to the Env-expressing cell surface in the presence of sCD4 or a CD4 mimic are shown among gated PM1 cells along with a control antibody (anti-human CD19: black lines). Data are representative of the results from a minimum of two independent experiments. The number at the top of each graph shows the mean fluorescence intensity (MFI) of the antibody 4C11.

Table 2
Combination indices (CI) for compound **2** or sCD4 and a CXCR4 antagonist, T140, against an HIV IIIB strain

Combination	HIV strain	CI values at different IC[a]		
		IC_{50}	IC_{75}	IC_{90}
2 + T140	IIIB	0.786	0.713	0.655
sCD4 + T140	IIIB	0.705	0.528	0.400

[a] The multiple-drug effect analysis reported by Chou et al. was used to analyze the effects of combinational uses of compounds.[18] CI <0.9: synergy, 0.9 < CI < 1.1: additivity, CI >1.1: antagonism.

(Table 2).[15] Compound **2** showed a highly remarkable synergistic anti-HIV activity with a co-receptor CXCR4 antagonist, T140,[8a] against an X4-HIV-1 strain, IIIB at various IC values (IC_{50}, IC_{75} and IC_{90}). However, sCD4 exhibited a higher synergistic effect (lower CI values) with T140 (Table 2). The interaction of sCD4 or a CD4 mimic with gp120 would expose the co-receptor-binding site of gp120, and the co-receptor CXCR4 could then easily approach gp120. Thus, an inhibitory effect of a CXCR4 antagonist would be meaningful, and a significant synergistic effect might also be brought about by a combination of sCD4 or a CD4 mimic and T140.

In summary, a series of CD4 mimic compounds were synthesized and evaluated for their anti-HIV activity. Several compounds showed significant anti-HIV activity with relatively low cytotoxicity. SAR studies showed that a certain level of size and electron-withdrawing ability of the substituents at the *p*-position of the phenyl ring are suitable for potent anti-HIV activity. In addition, the treatment of Env-expressing cells with several CD4 mimicking compounds causes a conformational change, exposing the co-receptor-binding site of gp120 externally. Thus, a CD4 mimic exhibited a remarkable synergistic effect with a co-receptor antagonist. These compounds are essential probes directed to the dynamic supramolecular mechanism of HIV entry, and important leads for the cocktail therapy of AIDS.

Acknowledgments

This work was supported by Mitsui Life Social Welfare Foundation, Grant-in-Aid for Scientific Research from the Ministry of Education, Culture, Sports, Science, and Technology of Japan, and Health and Labour Sciences Research Grants from Japanese Ministry of Health, Labor, and Welfare.

References and notes

1. Mitsuya, H.; Erickson, J. In *Textbook of AIDS Medicine*; Merigan, T. C., Bartlett, J. G., Bolognesi, D., Eds.; Williams & Wilkins: Baltimore, 1999; pp 751–780.
2. Chan, D. C.; Kim, P. S. *Cell* **1998**, *93*, 681.
3. (a) Alkhatib, G.; Combadiere, C.; Broder, C. C.; Feng, Y.; Kennedy, P. E.; Murphy, P. M.; Berger, E. A. *Science* **1996**, *272*, 1955; (b) Choe, H.; Farzan, M.; Sun, Y.; Sullivan, N.; Rollins, B.; Ponath, P. D.; Wu, L.; Mackay, C. R.; LaRosa, G.; Newman, W.; Gerard, N.; Gerard, C.; Sodroski, J. *Cell* **1996**, *85*, 1135; (c) Deng, H. K.; Liu, R.; Ellmeier, W.; Choe, S.; Unutmaz, D.; Burkhart, M.; Marzio, P. D.; Marmon, S.; Sutton, R. E.; Hill, C. M.; Davis, C. B.; Peiper, S. C.; Schall, T. J.; Littman, D. R.; Landau, N. R. *Nature* **1996**, *381*, 661; (d) Doranz, B. J.; Rucker, J.; Yi, Y. J.; Smyth, R. J.; Samson, M.; Peiper, S. C.; Parmentier, M.; Collman, R. G.; Doms, R. W. *Cell* **1996**, *85*, 1149; (e) Dragic, T.; Litwin, V.; Allaway, G. P.; Martin, S. R.; Huang, Y.; Nagashima, K. A.; Cayanan, C.; Maddon, P. J.; Koup, R. A.; Moore, J. P.; Paxton, W. A. *Nature* **1996**, *381*, 667.
4. Feng, Y.; Broder, C. C.; Kennedy, P. E.; Berger, E. A. *Science* **1996**, *272*, 872.
5. Wild, C. T.; Greenwell, T. K.; Matthews, T. J. *AIDS Res. Hum. Retroviruses* **1993**, *9*, 1051.
6. (a) Dorr, P.; Westby, M.; Dobbs, S.; Griffin, P.; Irvine, B.; Macartney, M.; Mori, J.; Rickett, G.; Smith-Burchnell, C.; Napier, C.; Webster, R.; Armour, D.; Price, D.; Stammen, B.; Wood, A.; Perros, M. *Antimicrob. Agents Chemother.* **2005**, *49*, 4721; (b) Price, D. A.; Armour, D.; De Groot, M.; Leishman, D.; Napier, C.; Perros, M.; Stammen, B. L.; Wood, A. *Bioorg. Med. Chem. Lett.* **2006**, *16*, 4633.
7. (a) Cahn, P.; Sued, O. *Lancet* **2007**, *369*, 1235; (b) Grinsztejn, B.; Nguyen, B.-Y.; Katlama, C.; Gatell, J. M.; Lazzarin, A.; Vittecoq, D.; Gonzalez, C. J.; Chen, J.; Harvey, C. M.; Isaacs, R. D. *Lancet* **2007**, *369*, 1261.
8. (a) Tamamura, H.; Xu, Y.; Hattori, T.; Zhang, X.; Arakaki, R.; Kanbara, K.; Omagari, A.; Otaka, A.; Ibuka, T.; Yamamoto, N.; Nakashima, H.; Fujii, N. *Biochem. Biophys. Res. Commun.* **1998**, *253*, 877; (b) Fujii, N.; Oishi, S.; Hiramatsu, K.; Araki, T.; Ueda, S.; Tamamura, H.; Otaka, A.; Kusano, S.; Terakubo, S.; Nakashima, H.; Broach, J. A.; Trent, J. O.; Wang, Z.; Peiper, S. C. *Angew. Chem., Int. Ed.* **2003**, *42*, 3251; (c) Tanaka, T.; Nomura, W.; Narumi, T.; Esaka, A.; Oishi, S.; Ohashi, N.; Itotani, K.; Evans, B. J.; Wang, Z.; Peiper, S. C.; Fujii, N.; Tamamura, H. *Org. Biomol. Chem.* **2009**, *7*, 3805.
9. Otaka, A.; Nakamura, M.; Nameki, D.; Kodama, E.; Uchiyama, S.; Nakamura, S.; Nakano, H.; Tamamura, H.; Kobayashi, Y.; Matsuoka, M.; Fujii, N. *Angew. Chem., Int. Ed.* **2002**, *41*, 2937.
10. (a) Zhao, Q.; Ma, L.; Jiang, S.; Lu, H.; Liu, S.; He, Y.; Strick, N.; Neamati, N.; Debnath, A. K. *Virology* **2005**, *339*, 213; (b) Schön, A.; Madani, N.; Klein, J. C.; Hubicki, A.; Ng, D.; Yang, X.; Smith, A. B., III; Sodroski, J.; Freire, E. *Biochemistry* **2006**, *45*, 10973; (c) Madani, N.; Schön, A.; Princiotto, A. M.; LaLonde, J. M.; Courter, J. R.; Soeta, T.; Ng, D.; Wang, L.; Brower, E. T.; Xiang, S.-H.; Do Kwon, Y.; Huang, C.-C.; Wyatt, R.; Kwong, P. D.; Freire, E.; Smith, A. B., III; Sodroski, J. *Structure* **2008**, *16*, 1689; (d) Haim, H.; Si, Z.; Madani, N.; Wang, L.; Courter, J. R.; Princiotto, A.; Kassa, A.; DeGrace, M.; McGee-Estrada, K.; Mefford, M.; Gabuzda, D.; Smith, A. B., III; Sodroski, J. *ProS Pathogens* **2009**, *5*, 1.
11. The structure of compound **2** was built in Sybyl and minimized with the MMFF94 force field and partial charges. (see: Halgren, T. A. *J. Comput. Chem.* **1996**, *17*, 490.) Docking was then performed using FlexSIS through its SYBYL

module, into the crystal structure of gp120 (PDB, entry 1RZJ). The binding site was defined as residues Val^{255}, Asp^{368}, Glu^{370}, Ser^{375}, Ile^{424}, Trp^{427}, Val^{430} and Val^{475}, and included residues located within a radius 4.4 Å. The ligand was considered to be flexible, and all other options were set to their default values. Figures were generated with ViewerLite version 5.0 (Accelrys Inc., San Diego, CA).

12. *For example, the synthesis of compound* **7**: To a solution of ethyl oxalyl chloride (0.400 mL, 3.48 mmol) in THF (20 mL) were added triethylamine (Et_3N) (0.480 mL, 3.48 mmol) and *p*-toluidine (373 mg, 3.48 mmol) with stirring at 0 °C. The reaction mixture was allowed to warm to room temperature, and then stirred for 6 h. After removal by filtration of the resulting salts, the filtrate was concentrated under reduced pressure. The residue was extracted with EtOAc (50 mL), and the extract was washed successively with brine (20 mL), 1 M HCl (20 mL × 2), brine (20 mL), saturated $NaHCO_3$ (20 mL × 2) and brine (20 mL × 3), then dried over $MgSO_4$. Concentration under reduced pressure gave the crude ethyl oxalamate, which was used without further purification. To a solution of the crude ethyl oxalamate (640 mg, 3.09 mmol) in THF (30 mL) were added aqueous 1 M NaOH (3.40 mL, 3.40 mmol), water (50 mL) and MeOH (20 mL) with stirring at 0 °C. The reaction mixture was allowed to warm to room temperature, and then stirred for 20 h. After the addition of aqueous 1 M HCl (5 mL), MeOH and THF were evaporated under reduced pressure. The residue was acidified to pH 2 with 1 M HCl, and extracted with EtOAc (50 mL × 2). The combined organic layer was washed with brine (20 mL × 3), and dried over $MgSO_4$. Concentration under reduced pressure gave the crude acid, which was used for the next reaction without further purification. To a solution of the above crude acid (514 mg, 2.87 mmol) in THF (10 mL) were added 1-hydoxybenzotriazole (484 mg, 3.16 mmol), 4-amino-2,2,6,6-tetramethylpiperidine (446 μL, 2.58 mmol), 1-ethyl-3-(3-dimethylaminopropyl)carbodiimide hydrochloride (606 mg, 3.16 mmol) and Et_3N (0.439 mL, 3.16 mmol) with stirring at 0 °C. The reaction mixture was allowed to warm to room temperature, and then stirred for 20 h. After evaporation of THF, the residue was dissolved in $CHCl_3$ (50 mL). The mixture was washed with saturated $NaHCO_3$ (20 mL × 2) and brine (20 mL × 3), and dried over $MgSO_4$. Concentration under reduced pressure gave the crude crystalline mass. The usual work-up followed by recrystallization from EtOAc–*n*-hexane gave the title compound **7** (363 mg, 1.14 mmol, 39.8%) as colorless crystals, mp = 176 °C; δ_H (400 MHz; $CDCl_3$) 1.07 (1H, m, NH), 1.16 (6H, s, CH_3), 1.29 (6H, s, CH_3), 1.44 (2H, m, CH_2), 1.91 (1H, d, *J* 3.7, C*H*H), 1.94 (1H, d, *J* 3.7, CH*H*), 2.34 (3H, s, CH_3), 4.25 (1H, m, CH), 7.17 (2H, d, *J* 8.3, ArH), 7.33 (1H, m, NH), 7.50 (2H, d, *J* 8.4, ArH), 9.18 (1H, s, NH); HRMS (FAB), *m*/*z* calcd for $C_{18}H_{28}N_3O_2$ $(MH)^+$ 318.2182, found 318.2173.
13. McFarland, C.; Vicic, D. A.; Debnath, A. K. *Synthesis* **2006**, 807.
14. *The synthesis of compound* **12**: To a solution of Et_3N (417 μL, 3.00 mmol) and 4-nitroaniline (138 mg, 1.00 mmol) in THF (1.3 mL) was added oxalyl dichloride (85.8 μL, 1.00 mmol) with stirring at 0 °C. After being stirred for 30 min at 0 °C, Et_3N (167 μL, 1.20 mmol) and 4-amino-2,2,6,6-tetramethylpiperidine (156 μL, 0.90 mmol) were added. The reaction mixture was stirred for 6 h at 0 °C. After removal by filtration of the resulting salts, the filtrate was concentrated under reduced pressure. The residue was dissolved in $CHCl_3$ (20 mL), and the mixture was washed successively with brine (10 mL), saturated $NaHCO_3$ (10 mL × 2) and brine (10 mL × 3), and dried over $MgSO_4$. Concentration under reduced pressure followed by flash chromatography over silica gel with $CHCl_3$–MeOH (9:1) gave 42.4 mg (0.122 mmol, 13.5%) of the title compound **12** as colorless crystals, mp = 190 °C; δ_H (400 MHz; $CDCl_3$) 1.09 (1H, m, NH), 1.17 (6H, s, CH_3), 1.29 (6H, s, CH_3), 1.43 (2H, m, CH_2), 1.92 (1H, d, *J* 3.8, C*H*H), 1.95 (1H, d, *J* 3.8, CH*H*), 4.28 (1H, m, CH), 7.29 (1H, m, NH), 7.82 (2H, d, *J* 9.1, ArH), 8.28 (2H, d, *J* 9.1, ArH), 9.55 (1H, s, NH); HRMS (FAB), *m*/*z* calcd for $C_{17}H_{25}N_4O_4$ $(MH)^+$ 349.1876, found 349.1871.
15. Yoshimura, K.; Shibata, J.; Kimura, T.; Honda, A.; Maeda, Y.; Koito, A.; Murakami, T.; Mitsuya, H.; Matsushita, S. *AIDS* **2006**, *20*, 2065.
16. (a) Chapman, N. B.; Shorter, J. *Advances in Linear Free Energy Relationship*; Plenum Press: London, 1972; (b) Chapman, N. B.; Shorter, J. *Correlation Analysis in Chemistry*; Plenum Press: London, 1978; (c) Hansch, C.; Leo, A. J.; Hoekman, D. *Exploring QSAR, Hydrophobic, Electronic, and Steric Constants*; American Chemical Society: Washington, DC, 1995.
17. Taft, R. W. In *Steric Effects in Organic Chemistry*; Newman, M. S., Ed.; John Wiley: New York, 1956; p 556.
18. (a) Chou, T. C.; Talalay, P. *J. Biol. Chem.* **1977**, *252*, 6438; (b) Chou, T. C.; Hayball, M. P. *CalcuSyn*, 2nd ed.; Biosoft: Cambridge, UK, 1996.

THE JOURNAL OF BIOLOGICAL CHEMISTRY VOL. 286, NO. 12, pp. 10581–10592, March 25, 2011

Single Particle Tracking Confirms That Multivalent Tat Protein Transduction Domain-induced Heparan Sulfate Proteoglycan Cross-linkage Activates Rac1 for Internalization*[S]

Received for publication, October 7, 2010, and in revised form, December 8, 2010 Published, JBC Papers in Press, January 3, 2011, DOI 10.1074/jbc.M110.187450

Junji Imamura[‡], Yasuhiro Suzuki[‡1], Kohsuke Gonda[§], Chandra Nath Roy[‡], Hiroyuki Gatanaga[¶], Noriaki Ohuchi[§‖], and Hideo Higuchi[**]

From the Departments of [‡]Emerging Infectious Diseases and [§]Nano-Medical Science, Graduate School of Medicine, Tohoku University, Seiryo-machi, Aoba-ku, Sendai 980-8575, the [¶]AIDS Clinical Center, International Medical Center of Japan, Toyama, Shinjuku-ku, Tokyo 162-8655, the [‖]Department of Surgical Oncology, Graduate School of Medicine, Tohoku University, Seiryo-machi, Aoba-ku, Sendai 980-8574, and the [**]Department of Physics, Graduate School of Science, University of Tokyo, Hongo Bunkyou-ku Tokyo 113-8654, Japan

The mechanism by which HIV-1-Tat protein transduction domain (TatP) enters the cell remains unclear because of an insufficient understanding of the initial kinetics of peptide entry. Here, we report the successful visualization and tracking of TatP molecular kinetics on the cell surface with 7-nm spatial precision using quantum dots. Strong cell binding was only observed with a TatP valence of ≥8, whereas monovalent TatP binding was negligible. The requirement of the cell-surface heparan sulfate (HS) chains of HS proteoglycans (HSPGs) for TatP binding and intracellular transport was demonstrated by the enzymatic removal of HS and simultaneous observation of two individual particles. Multivalent TatP induces HSPG cross-linking, recruiting activated Rac1 to adjacent lipid rafts and thereby enhancing the recruitment of TatP/HSPG to actin-associated microdomains and its internalization by macropinocytosis. These findings clarify the initial binding mechanism of TatP to the cell surface and demonstrate the importance of TatP valence for strong surface binding and signal transduction. Our data also shed light on the ability of TatP to exploit the machinery of living cells, using HSPG signaling to activate Rac1 and alter TatP mobility and internalization. This work should guide the future design of TatP-based peptides as therapeutic nanocarriers with efficient transduction.

A small region of HIV-1 Tat (*trans*-acting activator of transcription), corresponding to residues ^{47}YGRKKRRQRRR^{57} and the Tat protein transduction domain (TatP),[2] is responsible for translocating the protein across the cellular membrane (1–7). Several studies have reported the strong protein transduction property of these short sequences after fusion with various proteins both *in vivo* and *in vitro* (4, 6, 8). This property makes them extraordinarily good candidates for the transport of therapeutic bioactive molecules, such as proteins, DNA, RNA, or drugs, into cells. Therefore, understanding the molecular mechanisms of TatP entry and its efficacy is particularly important (3).

The pathway by which these peptides enter cells is the subject of substantial controversy (3). Biological assays have shown that TatP can enter into the cells at a relatively low concentration (~5 nM) (1, 9). In live cell imaging studies, photobleaching of GFP- and FITC-labeled TatP has been used to explore the mechanisms of TatP entry. The high concentrations (~10 μM to 100 nM) of TatP used in these experiments could induce the nonspecific entry of TatP into cells, however (5, 10–12). Therefore, it has been difficult to determine specific pathways. Moreover, because of the lack of state-of-the-art techniques for direct visualization, the initial events at the cell surface have only been predicted based on biological activities (*e.g.* activity of the reporter genes) or the amount of TatP inside the cells after ~1 h of TatP exposure. For instance, in a recently published paper (13), TatP was shown to enter cells in both pinosomes and macropinosomes after initially binding to an unidentified, non-HSPG protein. Pinocytosis is always occurring at the cell surface, even without stimulation. Increasing the TatP concentration might accelerate this nonspecific entry and prevent the discovery of a truly specific entry pathway (13). Thus, it is rather difficult to determine specific entry pathways using conventional live cell imaging and photobleaching fluorophores. There is still considerable controversy surrounding the validity of the data that have been obtained using such indirect measurements. As a result, phosphate groups of plasma membrane lipids (14–16) or cell-surface receptors, namely CXCR4 (17), integrin family members (18, 19), vascular endothelial growth factor receptor (20), low density lipoprotein receptor-related protein (21), and heparan sulfate (HS) proteoglycans (HSPGs) (10–12), are still considered potential candidates.

* This work was supported by a grant-in-aid for AIDS research from the Ministry of Health, Labor, and Welfare of Japan and by the Japanese Foundation for AIDS Prevention (to Y. S.).

[S] The on-line version of this article (available at http://www.jbc.org) contains supplemental "Experimental Procedures," Figs. S1–S7, and Videos 1–8.

[1] To whom correspondence should be addressed. Tel.: 81-022-717-8220; Fax: 81-022-717-8221; E-mail: suzukiy39@med.tohoku.ac.jp.

[2] The abbreviations used are: TatP, Tat-protein transduction domain; HS, heparan-sulfate; HSPG, HS-proteoglycan; QD, quantum dot; St, streptavidin; Ch, chondroitinase; DIC, differential interference contrast; MFI, mean fluorescent intensity; GPI, glycosylphosphatidylinositol-anchored; GAG, glycosaminoglycan; LatB, latrunculin-B; MBC, methyl-β-cyclodextrin; MSD, mean square displacement; val, valent; TatR, TatP Receptor.

Imaging of Tat Protein Transduction Domain in Living Cells

To clarify and quantify the mechanisms of TatP entry while overcoming the above-mentioned difficulties, we visualized the initial TatP molecular binding kinetics using a high speed confocal microscope and a high sensitivity camera with 7-nm spatial precision (22, 23). We used TatP labeled with quantum dots (QD), which are bright and resistant to photobleaching (24, 25). We were able to directly visualize and quantitatively analyze the initial molecular dynamics of TatP at the cell surface. Notably, we confirmed that multivalent TatP-induced HSPG cross-linking activates Rac1 for TatP internalization.

EXPERIMENTAL PROCEDURES

Reagents—St-QDs and biotinylated Alexa were purchased from Invitrogen. Unless otherwise mentioned, inhibitors of cellular proteins were acquired from Sigma. The Rac1 inhibitor NSC23766 was purchased from Calbiochem. mAb clone F58-10E4 (IgM class) (26), F69-3G10 (IgG_{2b} class) HS lyase, and Ch-ABC lyase were received from Seikagaku Corp. (Tokyo, Japan). Heparin was purchased from Sigma. We received the vector for glycosylphosphatidylinositol-linked GFP (pGFP-GPI) as a kind gift from Dr. Santos Manes (Centro Nacional de Biotechnologia/CSIC, Madrid, Spain) (27). The pAcGFP1-*tubulin* vector was purchased from Clontech.

Preparation of TatP-QDs—The 11-amino acid TatP sequence was synthesized by Fmoc (*N*-(9-fluorenyl)methoxycarbonyl) solid phase synthesis. The N terminus was conjugated with FITC or biotin or left unmodified. The peptides were purified by reverse phase-HPLC to >95% purity on an acetonitrile/H_2O/trifluoroacetic acid gradient and confirmed by electrospray ionization mass spectrometry (Toray, Osaka, Japan). The lyophilized peptides were reconstituted in distilled water to 3 mM stock concentrations. For the labeling of TatP with QDs, biotin-TatP was incubated with streptavidin (St)-QD (1 μM) at room temperature for 30 min at a TatP to St-QD molar excess of 1, 2, 4, 6, 8, 10, 12, and 16. To saturate the free Sts on the QDs, TatP-QDs were further incubated with an equal volume of 20 μM biotin at room temperature for 30 min. St-QD605s were used unless otherwise mentioned. The conjugated QDs were diluted in phenol red-free (Ph^-) X-VIVO-10 buffer (X-B) (Lonza, Walkersville, MD) for 45 min before the experiments.

Cell Culture and Drug Treatments—The cells were cultured in minimal essential medium (Invitrogen) with 10% FBS (Invitrogen) at 37 °C in 5% CO_2. 24 h before the start of the experiment, cells were detached and suspended at 1×10^5 cells/ml by Ph^- minimal essential medium with 10% FBS. Subsequently, 100- or 30-μl aliquots were plated onto either 96- or 384-well microwell plates (Nalge Nunc, Naperville, IL), which were coated with 15-fold-diluted Ph^- Matrigel Matrix (BD Biosciences) for 1 h and cultured overnight. One h before the microscopy experiments, the culture medium was exchanged for Ph^- X-B with 2% FBS. TatP-QD molecular imaging was performed at 37 °C on the microscope. Primary cells were isolated from a healthy donor and cultured as described previously (28).

The partial depletion of cholesterol from the plasma membrane was performed by incubating the cells in 4 mM methyl-β-cyclodextrin (MBC) at 37 °C for 30 min (29). This treatment did not decrease the surface expression of HSPG, which was followed by F58-10E4 with flow cytometry (data not shown). Partial actin depolymerization was performed by incubating the cells in medium containing 50 nM latrunculin-B (LatB) for 10 min at 37 °C (29). Rac1 was inhibited by treating the cells with 100 μM NSC23766 for 30 min at 37 °C. The Na^+/H^+ exchange and dynamin required for macropinocytosis were inhibited by treating the cells with 1 mM amiloride and 17 μM Dynasore, respectively, for 30 min at 37 °C.

Optical System for Single Molecule Imaging—The optical system that was used to observe the individual particles consisted of an epifluorescence microscope (IX-71, Olympus, Tokyo, Japan) equipped with a Nipkow lens-type confocal unit (CSU10, Yokokawa, Tokyo, Japan) and an electron multiplier type charge-coupled device camera (EM-CCD, Ixon DV887, Andor Technology, Belfast, Northern Ireland), as described previously (22, 30). A ×100 objective lens (UPlanFLN, 1.30 NA, oil, Olympus) was used. A 50×50 μm^2 area was illuminated with a green laser (532 nm wavelength, 50 milliwatts, CrystaLaser, Reno, NV). The laser-excited fluorescence was filtered with a >580 nm long pass filter to image the QDs. All images were processed with SOLIS software (Andor Technology). The position of a given QD was determined by fitting the image with two-dimensional Gaussian functions (30). As shown in Fig. 1*A*, immobile 8-val TatP-QDs on HeLa cells were tracked with a time resolution of 23 ms/frame; the standard deviation of the position of the QDs was 6.9 nm in the *x* axis and 6.5 nm in the *y* axis, indicating that the spatial precision for detecting TatP-QDs on HeLa cells was ~7 nm.

Dual Imaging for HSPG and TatP—For dual labeling of HSPG and TatP, the cells were detached with 0.25% trypsin/EDTA (Invitrogen), washed thoroughly with Ph^- X-B, and cultured for 6 h in 1.5 ml of Eppendorf tubes with X-B containing 2% FBS. Cultured HeLa cells were first incubated with mAb F58-10E4 (1:200) in PBS with 2% FBS (designated as the binding buffer, binding B) followed by a secondary goat anti-mouse IgM tagged with QD705 (1:100, Sigma). QD705-labeled anti-mouse IgM was prepared with a QD705 antibody conjugate kit (Invitrogen), according to the manufacturer's instructions. After labeling, the cells were incubated with 30 pM of 8-val TatP-QD525 for 10 min at room temperature and washed thoroughly with X-B. The cells were suspended at a concentration of 1×10^5 cell/ml in Ph^- X-B containing 2% FBS, plated on 96-well glass bottom plates (Nalge Nunc), centrifuged at 4 °C, and then observed under the microscope. QD525 and QD705 were illuminated with a blue laser (488 nm wavelength, 40 milliwatts, Furukawa Electric, Chiba, Japan). The laser-excited fluorescence was split into two paths with a dichroic mirror (transmission/reflection at 570 nm, Olympus, Tokyo, Japan) and filtered with a 500–550-nm bandpass filter for QD525 and a 690–730-nm bandpass filter for QD705 (22, 23, 31, 32). Images were taken at a rate of 200 ms/frame at 37 °C on the microscope.

Measurements of Individual Trajectories and Equations for Single Particle Tracking—The number of TatP-QDs bound to the cell and the dynamics of the QDs were examined by imaging at 400 and 23 ms/frame, respectively. TatP-QD cell-surface binding requires more than 10 min to plateau, so the lower rate of 400 ms/frame was used to avoid collecting unnecessarily large amounts of data (at 23 ms/frame, ~19 gigabytes would be required to store the >198,000 pictures).

When captured by the EM-CCD camera, the brightness of a single QD particle was characterized by a Gaussian distribution, with a peak at the center and a concentric drop in intensity. This unique property can be used to estimate the physical location of a single QD particle with nanometer accuracy. The positions of individual particles and their trajectories were determined with a single particle tracking plug-in for Image J (View5D, which automatically detects the positions of fluorescence-labeled particles).

To investigate the dynamics of the particle, a mean square displacement (MSD) was calculated from the *x-y* coordinates of the position of the tracked particle, as described previously (30). The MSD values were defined by Equation 1,

$$\mathrm{MSD}(n\Delta t) = \frac{1}{N-n}\sum_{i=1}^{N-n}[(x_{i+n}-x_i)^2 + (y_{i+n}+y_i)^2] \quad \text{(Eq. 1)}$$

where x_i and y_i give the position within frame i, and N is the total number of frames. The time between frames is Δt, and $n\Delta t$ is the time interval over which the MSD is calculated. To calculate the diffusion coefficients (D) and the velocities (V), MSD values were fitted by Equation 2,

$$\mathrm{MSD}(\Delta t) = 4D\Delta t + V^2(\Delta t)^2$$
$$\lim_{t\to 0}\mathrm{MSD}(\Delta t) = 4D\Delta t \quad \text{(Eq. 2)}$$

Optical System for Differential Interference Contrast (DIC) and Three-dimensional Image Reconstruction—The DIC images and reconstructed three-dimensional images of live cells were collected with a Zeiss LSM 510-meta confocal laser scanning microscope (Carl Zeiss, Jena, Germany) with a Plan-Apochromatic 63 × 1.4 NA oil-immersion DIC objective (Carl Zeiss). Live cells were imaged at 10-s intervals at 37 °C in Ph^- X-B. To generate the three-dimensional reconstructions of cells exposed to 8-val TatP-QD for 1 h, overlapping image stacks (10–15 stacks per cell; thickness of each image: 0.45 μm) were recorded with a ×2.0 scan zoom. The DIC and three-dimensional reconstructions were imaged with the Zeiss LSM Image Browser version 32.

Analysis of TatP Binding by FACS—To examine the ability of TatP-QD655 of varying valences to bind the cell surface, detached HeLa cells were cultured in 1.5-ml Eppendorf tubes with X-B for 6 h and exposed to 5 nM of TatP-QD of various valences for 15 min, washed three times with ice-cold binding B, and kept on ice until analysis with a FACSCalibur flow cytometer (BD Biosciences).

Activated Rac1-Pulldown Assay—HeLa cells were serum-starved for 24 h prior to the experiment and exposed to 30 pM of either 2- or 8-val-TatP. At the first indicated time point, the exposed cells were washed once with ice-cold PBS and lysed. The lysates (500 μg each) were subjected to a Rac1-GTP pulldown assay with GST-human Pak1-protein binding domain, using the active Rac1 pulldown and detection kit (Thermo Scientific, Rockford, IL) and the manufacturer's instructions. Samples were loaded and blotted with anti-Rac1 mAb (1:3000) and an HRP-labeled anti-mouse IgG (1:3000). Signal was visualized with SuperSignal West Pico chemiluminescent substrate (Thermo Scientific).

Enzymatic Treatment, HSPG Expression, and 8-val TatP Binding—To examine the cell-surface expression of HSPG, cells were detached and cultured in 1.5-ml Eppendorf tubes with X-B containing 2% FBS at least 6 h prior to experiments. Cells were stained with either anti-HSPG mAb (1:100) or an isotype-matched mAb followed by a FITC-conjugated secondary Abs (1:500) (Sigma). For experiments involving the enzymatic removal of the HS chains from cell-surface HSPGs by either HS lyase or Ch-ABC lyase, the cells were incubated for 2 h at 37 °C with HS lyase (20 milliunits) or Ch-ABC lyase (0.5 unit) in HS lyase buffer (20 mM Tris, pH 7.4, 0.01% BSA, and 4 mM $CaCl_2$) or Ch-ABC lyase buffer (3.3 mM Tris, pH 8.0, 0.01% BSA, 3.3 mM sodium acetate), respectively, and stained as described above. Aliquots of the enzyme-treated cells were plated and attached to 96-well glass bottom plates by centrifugation at 4 °C. The level of binding of 30 pM of 8-val TatP-QD to the HeLa cells was examined by single molecule microscopy as described above, with an acquisition rate of 200 ms/frame.

To study the effect of trypsin, cells treated with 0.25% trypsin/EDTA for 8 min were cultured in 1.5-ml Eppendorf tubes with X-B with 2% FBS. Trypsin/EDTA-treated cells were collected at the time indicated and examined for HSPG expression or 10 nM 8-val TatP-QD binding by FACS or 30 pM of 8-val TatP-QD binding by single molecule microscopy as described above.

RESULTS

Monovalent TatP Does Not Efficiently Bind to the Cell Surface—To visualize the interactions between TatP and the cell surface, we used St-QDs coupled with biotin-TatP at a TatP/QD molar ratio of 1:1. Unless otherwise stated, all experiments were conducted with the HeLa cell line. We cultured the HeLa cells on glass-bottom plates, exposed them to either 30 or 250 pM of TatP-QDs for 30 s, and observed them under a Nipkow-type confocal microscope at a time resolution of 400 ms/frame. TatP-QD molecules that are not bound to the surface move very rapidly due to Brownian motion, and at this rate of acquisition, these particles cannot be localized in discrete spots. Only QDs that are bound to the membrane can be recognized as fluorescent spots. As shown in Fig. 1*B*, TatP-QDs surprisingly did not bind to the cell surface (~100 cells examined) even after exposing the cells for about 15 min to 30 or 250 pM (data not shown) of QDs (the methods that were used to measure the QD numbers are described in the supplemental "Experimental Procedures"). This result suggests that monovalent TatP-QDs do not bind to the surface of HeLa cells at concentrations of 30 and 250 pM.

The entry of TatP occurs in living cells at a concentration of ~10 μM (5, 10–12). We speculated that increasing the TatP concentration in the medium could enhance their ability to bind the cells. Using high concentrations of QDs would lead to very high background fluorescence, however. Thus, we first exposed the cells to 30 pM TatP-QDs for ~3 min and then added unlabeled TatP at different concentrations in the medium. As shown in Fig. 1*B*, the addition of unlabeled TatP to

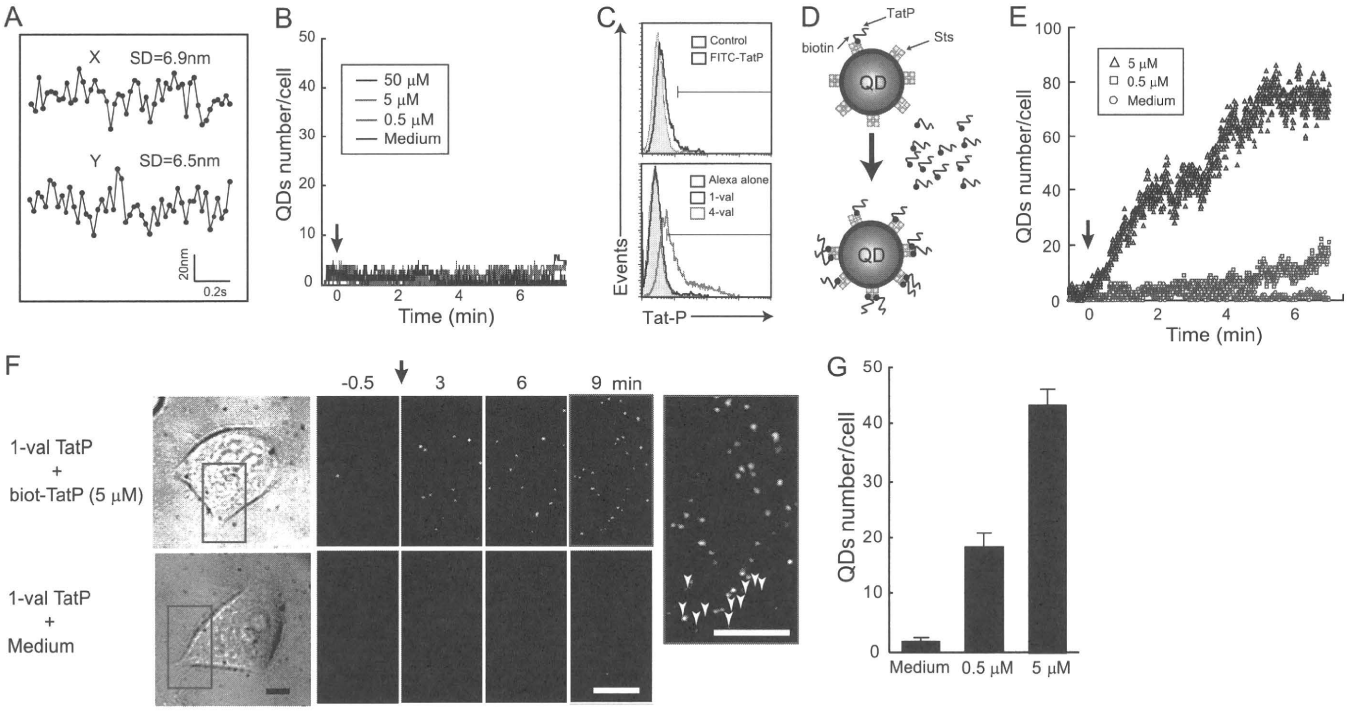

FIGURE 1. **Cell-surface binding of monovalent TatP.** *A*, spatial precision of TatP-QDs in HeLa. Immobile TatP-QDs were tracked in HeLa. The S.D. of the position of QDs was 6.9 nm in the *x* axis and 6.5 nm in the *y* axis. *B*, typical time course of monovalent TatP-QD cell binding to HeLa cells pre-exposed to 30 pM of monovalent Tat-QDs, followed by exposure to the indicated concentrations of nonlabeled TatP or medium. Data were collected at 400 ms/frame. *Arrow* indicates time of TatP addition. *C*, HeLa were exposed to either FITC-TatP, FITC alone (control) (*upper panel*), 1- and 4-val TatP-Alexa488, or Alexa488 alone (*lower panel*) for 15 min and analyzed for their binding capability by FACS. *D*, schematic figure illustrates the experiments for *E–G*: monovalent TatP-QD contains free sites for biotin-TatP on the Sts. *E* and *D*, typical time course of TatP-QD cell binding (*E*) and selected frames (*F*) from HeLa cells pre-exposed to 30 pM monovalent Tat-QDs, followed by exposure to the indicated concentrations of biotin-TatP. *Arrows* in *E* and *F* (*right panel*) indicate the time of biotin-TatP addition. *Bars*, 5 μm. *F*, *arrowheads* (*left panel*) indicate filopodia. *G*, mean QD number/cell calculated from ~20 cells exposed to biotin-TatP for 15 min. *Bars*, S.D. Results are representative of three independent experiments.

the medium at concentrations up to 50 μM does not significantly enhance the ability of TatP-QDs to bind the cell surface. Similarly, when FITC-labeled TatP was used to test surface binding, very little binding was observed after 15 min of exposure, as detected by FACS (Fig. 1*C*, *upper panel*). These results further confirm that monovalent TatP has little to no capacity to bind to the surface of HeLa cells. Because each St-QD typically contains ~7 streptavidin molecules, ~30 biotin-TatP molecules can bind to each St-QD. We studied the effect of adding biotin-TatP to the medium. We expected that the extra biotin-TatP would bind to the free streptavidin sites on the TatP-QDs (Fig. 1*D*). The cells were precultured with 30 pM monovalent TatP-QDs without added biotin (see "Experimental Procedures"), and different concentrations of biotin-TatP were then added to the medium. We found that the binding of TatP-QD to the cell surface, including filopodia, continually increased until a plateau was reached after ~5 min of biotin-TatP exposure (Fig. 1, *E* and *F*). The numbers of TatP-QD bound to the cell surface increased with increasing concentrations of biotin-TatP in the medium up to 5 μM (Fig. 1, *E* and *G*). These results suggest that the number of TatPs on the QDs could determine the capacity for cell-surface binding and that the TatPs in the medium interact with one another very little, if at all.

Multivalency of TatP Is Essential for Efficient Cell-surface Binding—To test whether the increase in TatP peptides per QD enhances cellular binding, we examined the cell surface association of QDs with different valences of TatP. One of the limitations of single molecule microscopy is that only a limited number of cells can be examined at once. Therefore, in addition to single molecule microscopy, we also employed FACS to analyze a larger population. We designate St-QD incubated with molar ratios of TatP/QDs of 1, 2–4, 6, 8, 10, 12, and 16 as 1-, 2-, 3-, 4-, 6-, 8-, 10-, 12-, and 16-valent (val) TatP-QD, respectively. Cells were incubated with these different valences of 30 pM TatP-QDs for 15 min and then placed on ice. The amount of TatP-QDs bound to the cellular surface was analyzed by FACS. As shown in Fig. 2 (*A* and *B*), the binding of TatP was found to increase as the valency increased from 4 to 8. The binding of ≥8-val TatP-QD was 15-fold higher than that of 4-val TatP-QD (Fig. 2*F*). At concentrations above 8-val, the binding did not further increase, as shown by both the relative mean fluorescence intensities (MFI) and the percentages of gated cells (data not shown). We studied the kinetics of 1-, 2-, 4-, 6-, 8-, 10-, 12-, and 16-val TatP and found that the cell-surface binding of 30 pM 8-val TatP-QDs was more rapid than that of 30 pM 4-val TatP-QDs (Fig. 2, *C–E*, and supplemental Video 1). The binding velocities of 2-, 4-, 6-, 12-, and 16-val TatP relative to that of 8-val TatP (as calculated from Fig. 1) were 10.1, 14.6, 35.1, 70.2, and 68.6%, respectively (Fig. 2*F*). We confirmed these results by testing the binding of different TatP valences, namely mono-, 2-, and 4-val TatP, labeled with St-Alexa488 (Fig. 1*C*, *lower panel*). The 4-val but not monovalent TatP showed a significant amount of binding after 15 min of exposure, as detected by

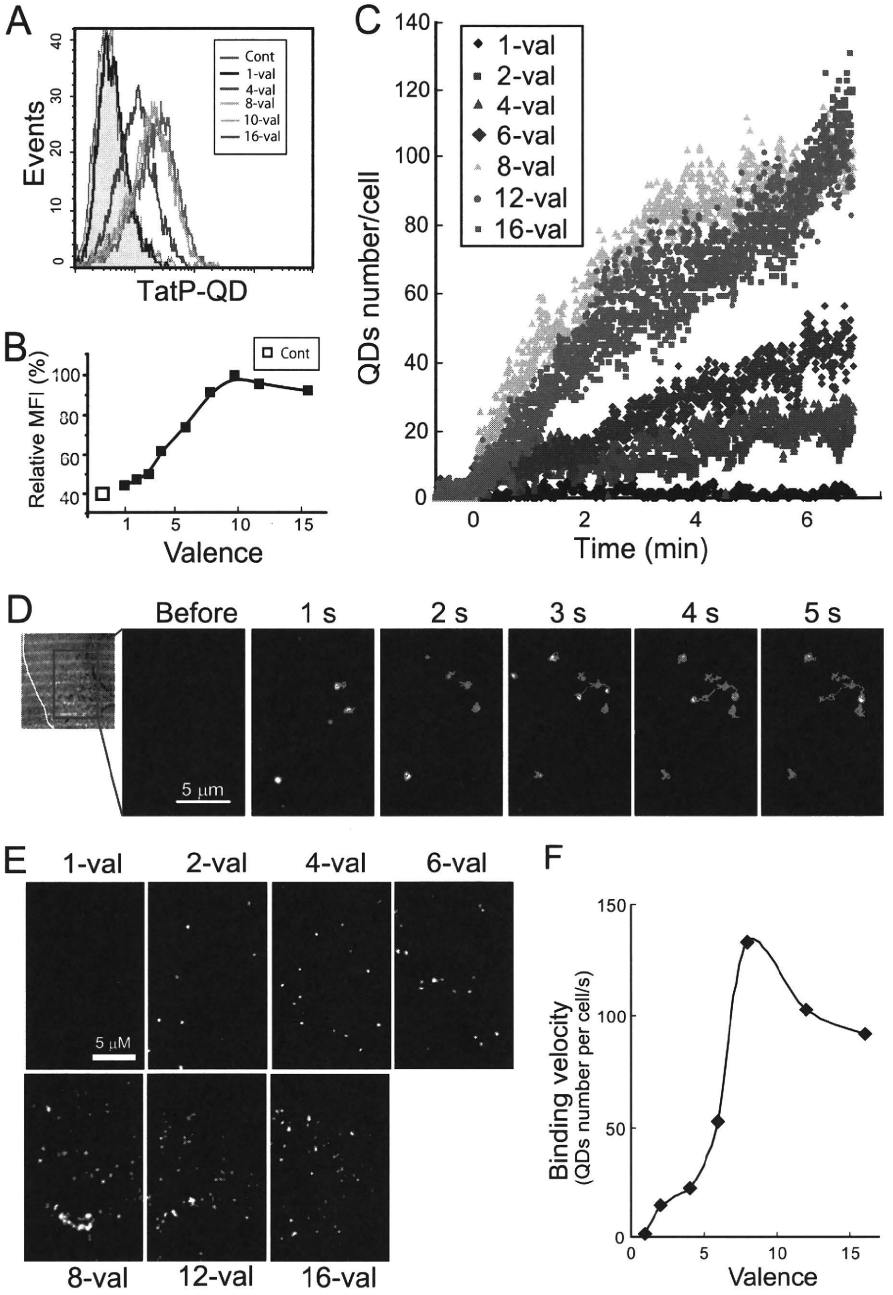

FIGURE 2. **Cell-surface binding of multivalent TatP.** *A* and *B*, analysis of cell-bound TatP of different valences in HeLa by FACS (*A*) and calculated relative MFI (*B*). Cells were exposed to TatP-QDs of the indicated valence or QDs alone (*cont*) for 15 min; binding levels were analyzed by FACS. *C* and *D*, typical time course of cell binding for TatP-QD of different valences to HeLa cells (*C*); images at 15 min of TatP exposure (*E*), and selected images of the first 5 s of 8-Val TatP cell exposure (*D*). The cells were exposed to TatP-QDs of the indicated valence or medium, and images were collected at 400 ms/frame. *Lines*, trajectories of the QDs. (See also supplemental Video 1.) *F*, binding velocities calculated from time course experiments in *C*. Results are representative of five independent experiments.

FACS (2.6 and 60.0% of cells bound mono- and 4-val-TatP$^+$, respectively). In addition, we found that 8-val TatP-QDs bound well to primary CD4$^+$T cells, macrophages, and B cells isolated from the peripheral blood cells of healthy donors (supplemental Fig. S1), suggesting that this phenomenon extends beyond HeLa cells.

Collectively, these results demonstrate that increasing the TatP valency on the QDs enhances cellular binding; we found that at least bivalent TatP-QD is required to support TatP-QD cell-surface binding on living cells, and a valence ≥8 is required for rapid and efficient cell-surface binding of TatP.

Multivalent TatP Remains on the Surface for About 20 min Before Internalization—We next examined whether the lower concentrations of cell surface-bound 8-val TatP-QD could translocate into the cells. We examined cultured HeLa cells exposed to 3 or 30 pM of 8-val TatP-QD for a 24-h period, obtaining confocal images at 30 and 40 min and 1, 2, and 24 h (supplemental Fig. S2*A*). We found that when the cells were exposed to 3 or 30 pM of 8-val TatP-QD, the number of QD particles attached to the cells was limited to either ~30 or ~400 of 8-val QD particles/cell 10 min after the addition of TatP. As reported previously (33), we found that TatP-QDs started to

appear inside the cells at 30 min; by 24 h essentially all of the TatP-QDs had accumulated in the perinuclear region. This region contains the microtubule organizing center, indicated by the co-localization of QDs with GFP-tubulin (data not shown). These results are consistent with the finding that the translocation of TatP that is mediated by either pinocytosis or endocytosis results in the formation of aggregates at the perinuclear region (33). Moreover, at 2 h after exposure, almost equal numbers of cell-bound TatP were internalized in the experiments containing 3 or 30 pM of 8-val TatP-QD (data not shown and Fig. 4*C*), indicating that ~250 bound TatPs are sufficient to induce the internalization of cell-bound QDs. Collectively, these results indicate that, after exposure to 3 or 30 pM of 8-val TatP-QD, TatP-QDs are successfully internalized into the cells.

We also measured how long the 8-val TatP-QDs remain on the cell surface before being internalized. To determine whether the cell surface-bound 8-val TatP-QDs were internalized after ~20 min of exposure, we examined the accessibility of the bound 8-val TatP-QDs to the external medium using two strategies. The first strategy was based on the finding that the TatP cell is mediated by electrostatic interactions and that membrane-bound TatP is easily removed by exposing the cells to an acidic buffer. We found that washing with 10 mM HCl in 150 mM NaCl caused immediate release of the QDs from the cell surface (supplemental Fig. S3*A*). With the second technique, we were able to avoid exposing the cells to the extremely low pH by exploiting the ability of QDs to serve as donors for fluorescence resonance energy transfer (FRET) (see supplemental "Experimental Procedures"). We used the cell-bound TatP-QD525 as a donor and a membrane-impermeable, biotinylated Alexa546 fluorophore as an acceptor (34). Because 8-val TatP-QD retains free biotin-binding sites, the addition of a membrane-impermeable, biotinylated fluorophore with an absorption peak corresponding to the QD emission band should result in FRET quenching only in those QDs that are accessible to the extracellular buffer and not yet internalized (supplemental Fig. S3*B*). As expected, the addition of the potential acceptor to the medium led to an immediate (within 1 s) and substantial (50–60%) quenching of QD525 on the cells after ~20 min of TatP exposure (supplemental Fig. S3, *C* and *D*). The amount of observed quenching was consistent with control experiments in which the acceptor was added to QD525 fixed to a glass slide. Collectively, these results indicate that most of the cell-bound 8-val TatP-QDs remains on the cell surface for at least ~20 min before internalization.

Signaling from Multivalent TatP Facilitates the Frequent and Constitutive Recruitment of TatP Receptor (TatR) to Actin-associated Membrane Lipid Rafts—Calorimetric analyses have revealed that TatP has a binding affinity for HS and induces the cross-linking and/or aggregation of HS-TatP complexes in the liquid medium (35). Thus, it is reasonable to hypothesize that multivalent TatP induces the cross-linking of HSPGs on the cell surface immediately after binding. To characterize the molecular behavior of TatP/TatR in the absence of cross-linking, we observed the movement of individual 2-val TatPs, which cannot induce the cross-linking of receptors, after 2, 5, and 15 min of exposure. To compare 2-val with 8-val TatP, we modified the concentration of 2-val TatP-QDs (300 pM) in the medium so that the number of attached QD particles (~400/cell) at ~15 min of exposure would equal that of the cells exposed to 30 pM 8-val TatP. We observed the movement of TatP-QDs on the cell surface at 23 ms/frame. The spatial precision at this time resolution is ~7 nm. As shown in Fig. 3*A*, 2-val TatP was found to exhibit apparently simple diffusion at 2 min after exposure; the mean diffusion coefficient (*mD*) in the 230-ms window, calculated from the constructed trajectories of single particles found in the images, was found to be 0.3 ± 0.06 $\mu m^2/s$ (mean ± S.E.; $n = 39$). For comparison, we also examined the mobility of CD4, a monomeric transmembrane protein, using CD4-expressing HeLa cells and QD705-labeled anti-CD4 Ab. CD4 exhibited almost identical behavior to that of 2-val TatP, $mD = 0.26 \pm 0.07$ ($n = 39$). The trajectory (Fig. 3*A*), proportion of mobility (Fig. 3*B*), and *mD* (Fig. 3*C*) values for 2-val TatP did not significantly change until 15 min ($mD = 0.28 \pm 0.05$ and 0.33 ± 0.04 after 5 and 15 min, respectively). We fit the intensity distributions of the visualized spots to multiple Gaussian curves and compared them with the distributions of a single QD. In so doing, we found that cell-bound 2-val TatP consists of single QD molecules after an exposure of 2 and 15 min (Fig. 3*D*, *upper panels*). Plasma membrane proteins are organized into microdomains that are compartmentalized by the membrane-bound actin cytoskeleton as well as the hydrodynamic slowing effects of transmembrane-protein pickets that are anchored on the membrane-skeleton fence (29, 36, 37). Thus, both the trajectory and the *mD* are sensitive parameters for detecting complex formation between proteins and the membrane skeleton. The behavior of 2-val TatP suggests that TatR initially exists as a monomer; the cell surface mobility of 2-val Tat does not significantly change over time.

We then observed the movement of each individual 8-val TatP to explore the effect of multiple TatPs on the induction of HSPG-cross-linking. The trajectory (Fig. 3*A*), the proportion of mobility (Fig. 3*B*), and the *mD* (Fig. 3*C*) of 8-val TatP particles were almost identical to those of 2-val TatP particles until 5 min. Thereafter, these parameters were found to drop substantially over time until 15 min ($mD = 0.31 \pm 0.04$ ($n = 39$), 0.23 ± 0.06 ($n = 56$), 0.17 ± 0.02 ($n = 99$) after 2, 5, 15 min, respectively) (Fig. 3, *A* and *C*, and supplemental Videos 2 and 3). In the presence of TatP, *de novo* binding to the cell surface continues throughout the observation; thus, the *mD* calculated under these conditions could be influenced by the mobility of recently cell-bound TatP. Thus, after exposing the cells to 8-val TatP for 2 min, the cells were washed to remove TatP from the medium. We found that by reducing the *mD* of 8-val TatP with the wash step, the mobility becomes more prominent ($mD = 0.15 \pm 0.03$ *versus* 0.23 ± 0.06 and 0.17 ± 0.02 *versus* 0.12 ± 0.03 after 5 and 15 min, respectively) (Fig. 3*E*). The intensity distributions of the cell-bound 8-val TatP particles were found to gradually increase, suggesting that they consisted of more than two QDs (see Fig. 3*D*, *lower left* and *middle panels*). We describe these spots in the rest of this paper as spots$_{>2\ QDs}$. We found that after partial actin depolymerization (by LatB) or partial cholesterol depletion (by MBC), diffusion of the 8-val TatP slows (0.172 ± 0.02 ($n = 100$), 0.347 ± 0.05 ($n = 104$), and 0.329 ± 0.02 ($n = 18$) in untreated, LatB, and MBC, respectively) (Fig.

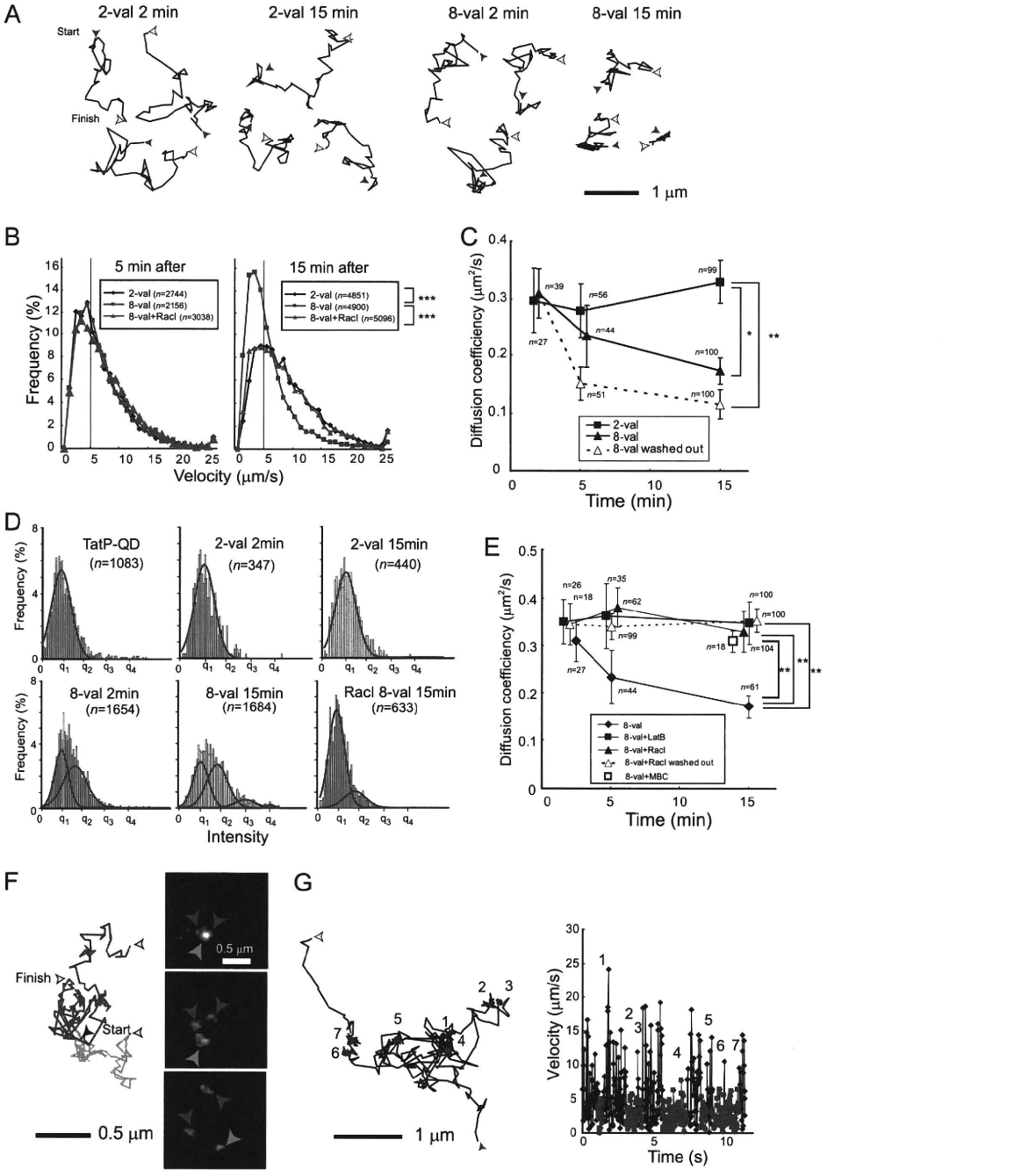

FIGURE 3. **Multivalent TatP induces a slowing of diffusion by frequent recruitment of TatR to actin-associated membrane lipid rafts.** *A*, typical trajectories of 2- or 8-val TatP after 2 and 15 min of exposure, recorded at 23 ms/frame. (See supplemental Videos 2 and 3.) *B*, histograms of 2- and 8-val-TatP velocities (calculated from 1150-ms time window) in the presence or absence of 100 μM Rac1 inhibitor after 5 min (*left*) and 15 min (*right*) of exposure. *C*, mean diffusion coefficient of 2- or 8-val TatP, over time up to 15 min, averaged for all particles in time window 1150 ms. Mean diffusion coefficient of 8-val TatP on cells, when unbound QDs were washed out after 2 min of exposure (8-val washed out). *Bars*, S.E. *D*, intensity histogram of TatP-QDs at the indicated time and condition, fitted to four gaussian curves. The mean of the first peak is equal to TatP-QD (*left upper panel*), defined as q_1. *E*, mean diffusion coefficient of 8-val TatP in the presence and absence of 50 nM LatB, 100 μM Rac1 inhibitor (RacI), and 4 mM MBC. *Bars*, S.E. *F*, selected frames (*left*) and trajectories of 8-val TatP-QDs from 23 ms/frame after a 15-min exposure. *Arrowhead* color corresponds to that of its trajectory. (See supplemental Video 4.) *G*, often 8-val TatP exhibited alternating periods of apparently simple Brownian diffusion (*black*) and temporary immobilization (*red*) for 500 frames (*left*). Changes in velocity of the trajectories over time are also shown (*right*). The numbers of temporal immobilizations of the trajectories correspond with the graph. (See also supplemental Video 5.) *, $p < 1 \times 10^{-5}$; **, $p < 1 \times 10^{-7}$; ***, $p < 1 \times 10^{-15}$ as calculated by Student's *t* test.

3*E*), and the spots$_{>2\ QDs}$ almost disappeared (data not shown). Thus, our results indicate that the slowing of 8-val TatP movement might be caused by the binding of TatP/TatR clusters to actin filaments and/or membrane-associated microdomains, as this rate decrease is affected by partial actin depolymerization. One might expect that the disruption of the membrane rafts and actin cytoskeleton might actually increase the freedom of TatP or the mobility of TatR across the cell membrane, thereby increasing the probability of aggregation between different TatP-QD-TatR complexes on the cell surface. We found, however, that the number of spots$_{>2\ QDs}$ does not increase with LatB treatment, suggesting that the TatP-QD-TatR complexes

do not easily aggregate with other complexes in the absence of polymerized actin. The reduction in the movement of the 8-val TatP particles and the increase in the number of spots$_{>2\ QDs}$ were also linked to cholesterol-rich domains in the membrane, known as lipid rafts or cholesterol-enriched membrane microdomains. Indeed, with HeLa cells expressing GFP-GPI, we found that 8-val TatP-QD co-localizes with GFP-GPI after ~20 min of exposure; FITC-GPI is used as a marker for membrane lipid rafts (supplemental Fig. S4). When we observed the spots$_{>2\ QDs}$ after 15 min of exposure, we found that they exhibit continuous association and dissociation mobility in a confined area (Fig. 3*F* and supplemental Video 4). Similarly, after 15 min of exposure, we noticed that only 8-val TatP particles often exhibit temporary immobilization in its trajectories (Fig. 3*G* and supplemental Video 5). These temporary pauses persisted for nearly half of the total observation time (67 of 138 s). The temporarily immobilized spots usually have velocities ≤ 5 μm/s (Fig. 3*G*, *right panel*), and the number of these spots is significantly higher in cells exposed to 8-val TatP than in those exposed to 2-val TatP after 15 min (34.2 *versus* 64.1% on cells exposed to 2-val and 8-val TatP, respectively). These temporary immobilization events were also inhibited by both partial depolymerization of the actin filaments and partial cholesterol depletion (data not shown). Notably, the reduced mobility and the temporary immobilization events of 8-val TatP are not directly linked to the internalization of TatP, as 8-val TatP remains on the cell surface for 15 min (supplemental Fig. S3). Moreover, those pauses are always temporary. Collectively, these results suggest that the cross-linked TatP on the higher valency QDs facilitate the frequent and constitutive recruitment of TatP/TatR to actin-associated membrane lipid raft microdomains through an unknown signal.

Multivalent TatP Activates Rac1 to Slow Molecular Movement and Induce Internalization through Macropinocytosis—Full-length Tat protein exposure activates Rac1, a GTP-binding protein that regulates membrane actin polymerization (19). Activated Rac1 also regulates membrane ruffling and macropinocytosis by reorganizing actin in growth factor-stimulated cells (34, 38, 39). Activated Rac1 was shown to be preferentially recruited to lipid rafts, triggering downstream signaling cascades (40, 41). We hypothesized that multivalent TatP induces the cross-linking of TatR, which causes the rearrangement of Rac1 adjacent to the lipid rafts and the membrane actin near the raft domains. In turn, TatR movement would be reduced, and TatP/TatR particles would be internalized by macropinocytosis. We first tested whether Rac1 was activated by TatP exposure with a pulldown assay that detects active GTP-bound Rac1 using the Rac1-GTP-binding domain of Pak1 (Fig. 4*A*) (40). We measured the amplitude and the time course of Rac1 activation in the cells exposed to 2-val and 8-val TatP and found that 8-val TatP-QDs activate Rac1 within 7 min of exposure, continuing until 15 min of exposure. In contrast, the induction of Rac1 activation was marginal in cells exposed to 2-val TatP. We also studied the mobility of individual 8-val QDs in cells pre-exposed to NCS23766, a Rac1 inhibitor. We found that reductions of *mD* (0.34 ± 0.05 (n = 18), 0.38 ± 0.04 (n = 35), and 0.33 ± 0.04 (n = 100) at 2, 5, and 15 min, respectively) and the induction of temporary immobilization events (the number of spots

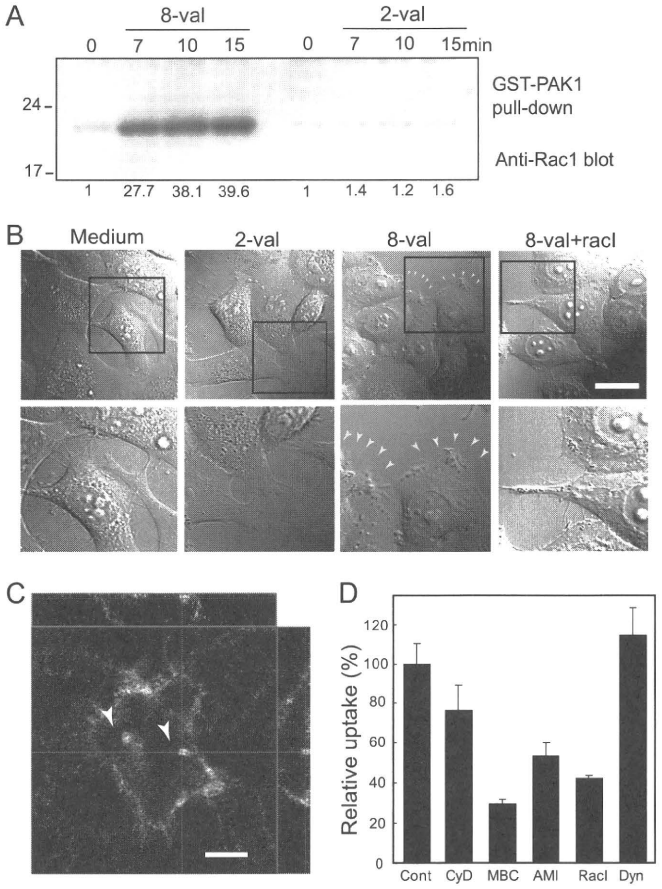

FIGURE 4. **Activation of Rac1 by 8-val-TatP exposure linked to membrane ruffling and TatP internalization by macropinocytosis.** *A*, levels of activated Rac1 after 8-val or 2-val TatP-QD exposure. HeLa cells, 24-h serum-starved, were exposed to 30 pM 8-val or 2-val TatP-QDs for the indicated times and lysed. Lysates were harvested, and Pak1 pulldown was performed. Samples from pulldowns were loaded and blotted with anti-Rac1. The *numbers* indicate the level of Rac1 activation. *B*, DIC images of HeLa cells at 15 min after 8-val TatP in the presence and absence of 100 μM Rac1 inhibitor, NCS23766 (*upper panel*). Higher magnitude images in *upper panel squares* are shown in *lower panels*. HeLa cells, 24-h serum-starved, were cultured with/without 100 μM Rac1 inhibitor (*Racl*) and exposed to 100 pM 8-val-TatP-QDs, and DIC images were collected every 10 s. A 2-val TatP QD stimulation is shown as a control. *Arrowheads* indicate prominent membrane ruffling. *Bar*, 20 μm. (See also supplemental Videos 6 and 7.) *C*, three-dimensional reconstructed images of a HeLa cell exposed to 100 pM 8-val TatP for 1 h. *Arrowheads* indicate TatP containing macropinosomes. *Bar*, 10 μm. *D*, effects of 50 nM cytochalasin D (*CyD*), 4 mM MBC, 1 mM amiloride (*AMI*), 100 μM Rac1 inhibitor (*Racl*), and 17 μM Dynasore (*Dyn*). Cells were exposed to the indicated drugs and exposed to 100 pM 8-val TatP for 1.5 h; images were collected by LSM510 confocal microscope at ~2 μm above the glass surface, which can identify cytoplasm. Uptake levels were calculated based on 20 observed cells. *Bars*, S.D. Results in *B–D* are representative of five independent experiments.

with a velocity <5 μm/s in Fig. 3*B* is 36.2%) were suppressed by NCS23766. The gradual increase in the number of the spots$_{>2\ QDs}$ over time was also found to be significantly suppressed by this inhibitor. Rac1 was found to cluster with TatP-coated beads and not uncoated beads (supplemental Fig. S5), confirming the effect of TatP on Rac1 targeting to the membrane. These findings suggest that the TatP-induced cross-linking of TatR activates Rac1 and that activated Rac1 is recruited to lipid raft domains (see supplemental Figs. S4 and S5). These events result in membrane actin reorganization, which ultimately slows and confines the cell-surface mobility of TatP/TatR. We then examined whether Rac1 activation by multiva-

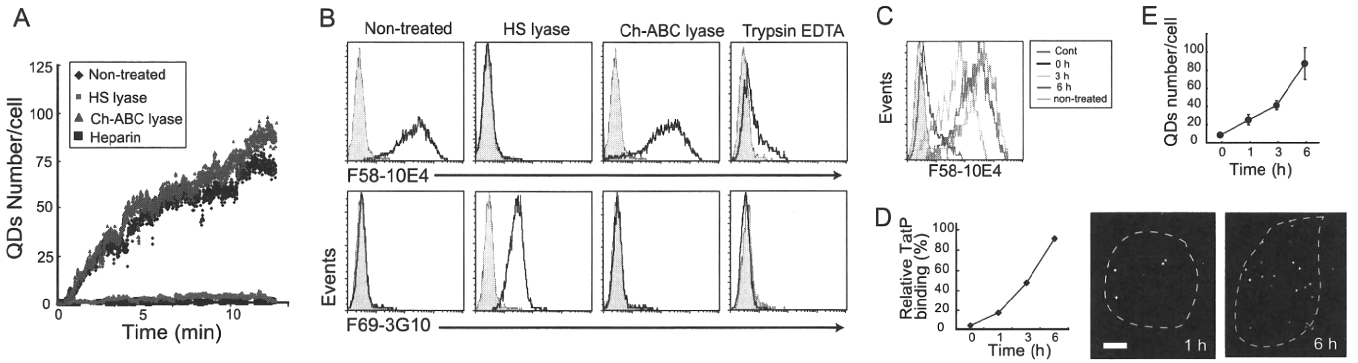

FIGURE 5. **HSPGs are essential for initial TatP cell-surface binding.** *A,* typical time course of monovalent TatP-QD cell binding to HeLa cells treated with 20 milliunits of HS lyase or 0.5 units of Ch-ABC lyase or cultured with 10 units of heparin. Images were collected at 400 ms/frame. *B,* binding of a mAb specific for intact HSPGs (F58-10E4) or for an epitope generated by the cleavage of HSPGs with HS lyase (F69-3G10). Cells were treated with 20 milliunits of HS lyase (*middle right panel*), 0.5 units of Ch-ABC lyase (*middle left panel*), or 0.5% trypsin/EDTA (*right panel*); nontreated cells (*left panels*) were stained with the indicated Abs and analyzed by FACS. *Dark lines* represent anti-HSPG Abs; *light lines* represent isotype-control. *C,* turnover of HSPG (F58-10E4) in cells treated with 0.5% trypsin/EDTA by FACS. *D,* recovery of the cell-surface binding capability of 8-val TatP-QDs in cells treated with 0.5% trypsin/EDTA. Data were calculated from the MFI values by FACS. *E,* recovery of the cell-surface binding capability of 8-val TatP calculated from single particle images of 8-val-TatP binding in cells treated with 0.5% trypsin/EDTA. The relative binding capability of 8-val TatP over time was calculated from the mean numbers of TatPs/cell based on 20 observed cells (*upper graph*) and selected images (*lower panels*). *Bars,* S.D. Results are representative of three independent experiments.

lent TatP is linked to the internalization of TatP/TatR. Rac1 activation correlates with membrane ruffling (29, 42). Thus, we first characterized the changes in cell shape in cells exposed to TatP using DIC images acquired at 1-min intervals for about 15 min. As shown in Fig. 4*B*, membrane ruffling was greatly enhanced in response to 8-val TatP exposure (see also supplemental Video 6). Moreover, three-dimensionally reconstructed images of the cells after ~1 h of 8-val TatP exposure revealed that the number of TatP-QD-containing vesicles had increased (Fig. 4*C*). These vesicles contain extracellular fluid, as determined by dye uptake in cells pulsed with Alexa488-dextran (supplemental Fig. S6). We examined the effect of the various inhibitors on 100 pM of 8-val TatP-QD internalization by focusing inside the cells at ~2 μm above the glass surface (the level at which transfected intracellular GFP can be easily visualized) (supplemental Fig. S2*B*). We found that the internalization of 8-val TatP is suppressed by inhibiting actin polymerization (cytochalasin D) and Na^+/H^+ exchange required for macropinocytosis (amiloride) and by changing cholesterol levels with MBC, as reported previously (9, 43). The inhibitor for dynamin (Dynasore), a GTPase responsible for most of the endocytotic pathways (44), had no effect (Fig. 4*D*). From these data, we can confidently assume that the exposure of cells to 8-val TatP induces the internalization of TatP through macropinocytosis. We next studied the effects of the Rac1 inhibitor. When cells were pre-exposed to NCS23766, both the enhancement of membrane ruffling (Fig. 4*B* and supplemental Video 7) and the induction of macropinocytosis were substantially suppressed (Fig. 4*D*). In addition, 2-val TatP did not induce membrane ruffling or macropinocytosis. In summary, multivalent (≥8 val) TatP induces the activation of Rac1, which leads to membrane actin reorganization and the reduction of TatP/TatR mobility. TatP recruits the activated Rac1 adjacent to cholesterol-rich domains and facilitates the internalization of TatP by macropinocytosis.

HSPGs Are Essential Receptors for TatP Cell-surface Binding—Several studies have shown that cell-surface HSPGs are involved in Tat transduction into cells (10–12). It is not clear, however, whether HSPGs are directly involved in the initial steps of Tat cell-surface binding. HSPG is composed of a core protein and ≥3 linear HS-glycosaminoglycan (GAG) polysaccharide chains (45). We first studied the effect of heparin (a highly sulfated GAG) on the cellular binding of TatP. HeLa cells were cultured in the presence or absence of 10 units of heparin, exposed to 30 pM of 8-val Tat, and observed by single molecule microscopy. As shown in Fig. 5*A*, the cell-surface binding of 8-val TatP was totally abrogated after the addition of heparin.

To clarify the involvement of HSPGs in the cell-surface binding of TatP, we examined the effect of removing cell-surface GAGs with specific enzymes. We used HS lyase, which cleaves GAG from HSPG, as well as chondroitinase (Ch)-ABC lyase, which cleaves the chondroitin sulfate chain from chondroitin sulfate proteoglycans. As expected, the binding of mAb F58-10E4, which specifically recognizes a GAG epitope of native HSPG, was reduced almost to background levels when HeLa cells were treated with 10 milliunits of HS lyase (Fig. 5*B*, *upper panels*). Conversely, F69-3G10, an HSPG epitope that is revealed after HS lyase treatment, did not bind to the untreated HeLa cells but bound to HS lyase-treated cells (Fig. 5*B*, *lower panels*). We examined the binding of 30 pM 8-val TatP to the enzyme-treated cell surface by single molecule microscopy. We found that the treatment with HS lyase, but not Ch-ABC lyase, totally abrogates 8-val TatP cell-surface binding to HeLa cells (Fig. 5*A*). This result suggests that the GAGs of HSPGs serve as the initial receptors for TatP on the cell surface.

We then examined the effect of trypsin, a serine protease that digests cell-surface proteoglycans (46). When cells were treated with 0.25% trypsin/EDTA, the binding of F58-10E4 was reduced almost to background levels, and F69-3G10 did not bind (Fig. 5*B*). This result suggests that HSPGs on the surface are depleted by trypsin. We observed rapid turnover of HSPGs after trypsin treatment, with the MFI levels of F58-10E4 returning to 47.8 and 98.5% of the normal levels after 3 h and 6 h, respectively (Fig. 5*C*). Accordingly, when trypsin-treated cells were exposed to 8-val TatP, the cellular binding of TatP was initially totally abrogated (Fig. 5, *D* and *E*), but binding was

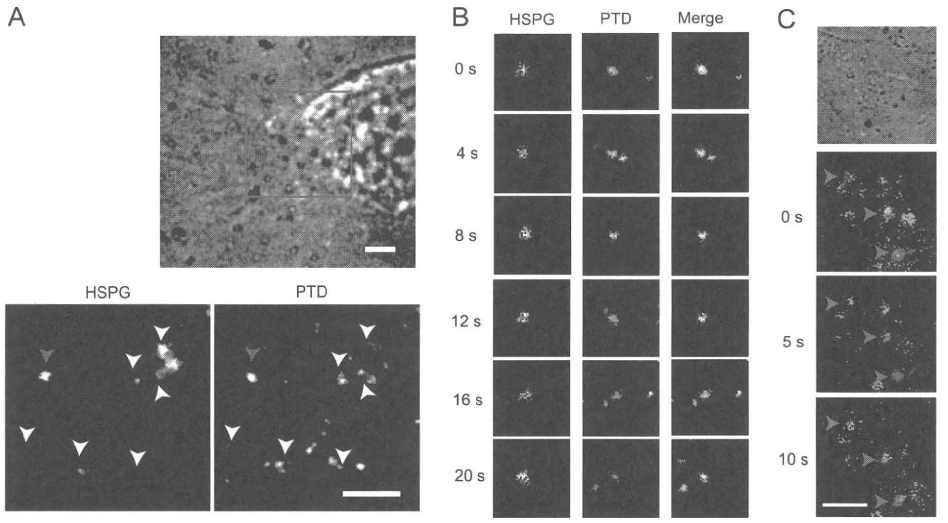

FIGURE 6. **Co-mobilization and co-internalization of TatP and HSPG.** *A*, bright field image (*upper panel*) and fluorescence images in the *red square* were obtained using dual imaging system (*lower panel*) at 200 ms/frame. Fluorescence images of TatP-QD525 (*lower left panel*) and HSPG as detected by F58-10E4 plus secondary Ab labeled with QD705 (*lower right panel*) at 20 min of TatP exposure. *Arrowheads* indicate co-localization spots of TatP and HSPG. *Bars*, 5 μm. *B*, time course fluorescence images of TatP and HSPG of the *red arrow* in *A*. (See also supplemental Video 8.) *C*, bright field image (*upper*) and selected frames of merged fluorescence images of TatP (*green*) and HSPG (*red*) at 45 min of TatP exposure. *Arrowheads* indicate co-localization of TatP and HSPG. Images are contrast-enhanced. *Bar*, 1 μm.

restored to ~50 and ~90% of normal levels within 3 h and 6 h, respectively. These results clearly demonstrate that the GAG chains of HSPGs, which are expressed on the cellular surface, serve as the initial cell-surface receptors for TatP.

TatP-HSPGs Co-mobilize in Living Cells—To confirm the role of HSPGs as receptors for TatP, we simultaneously observed two single particles of TatP and HSPGs in living cells using single molecule microscopy with the dual imaging techniques that have been previously developed and reported (22, 23, 30). To observe the movement of HSPGs and TatP, HeLa cells were first incubated with mAb F58-10E4 followed by QD705-labeled secondary Ab at 4 °C. The cells were subsequently incubated with 30 pM 8-val TatP-QD525 for 10 min, plated onto glass-bottom plates, centrifuged at 4 °C, and visualized at a time resolution of 200 ms/frame. As shown in Fig. 6 (*A* and *B*) (see also supplemental Video 8), after exposure for >30 s, 17.8% (n = 124) of the total TatP co-mobilized with HSPGs at the cellular surface at 20 min. We also observed that TatP-HSPGs were co-mobilized inside the cells within 45 min of 8-val TatP exposure (Fig. 6*C*). The percentage of TatP co-mobilized with HSPG appears to be much lower, but note that we had to use a much lower concentration of F58-10E4 to overcome the antibody occupancy of the binding domain of TatP (47). Hence, the number of F58-10E4-QD spots was lower than that of TatP. Combined with the result that the enzymatic removal of HSPGs totally abrogates TatP cell-surface binding, the dual imaging of these two single particles confirms that cell-surface HSPGs serve as the initial TatP receptors and that the TatP-HSPGs complex transports TatP inside HeLa cells.

Level of TatP Bound to the Surface Does Not Correlate with the Level of F58-10E4 Antigen Expressed in a Variety of Cell Types—We next examined whether a similar phenomenon occurs in the HOS and HepG2 cell lines. We studied the correlation between TatP binding and the expression of HSPG in these cell lines (Fig. 7*A*). We found that the MFIs of F58-10E4

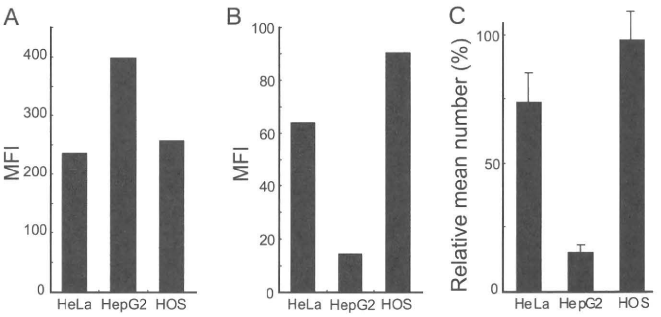

FIGURE 7. **Levels of HSPG expression and TatP-binding capability in various cell lines.** *A*, HSPG (as detected by F58-10E4) expression in HeLa, HepG2, and HOS by FACS. *B*, levels of 8-val TatP-QDs bound in HeLa, HepG2, and HOS as examined by FACS. *C*, relative mean number of 8-val TatPs/cell on different cells at 15 min of TatP exposure as observed by single molecule microscopy. Data are based on 20 observed cells. *Bars*, S.D.

mAb in HeLa, HepG2, and HOS were 235, 397, and 257, respectively. In contrast, the levels of 8-val TatP-QDs bound on the cellular surface, as detected with MFI in HeLa, HepG2, and HOS, were 64.1, 14.4, and 90.3, respectively (Fig. 7*B*). Moreover, the numbers of 8-val TatP-QDs, calculated by observing a mean of 10 cells each with single molecule microscopy in HeLa, HepG2, and HOS, were 74.6 ± 12.8, 17.2 ± 3.0, and 107 ± 23.6, respectively (Fig. 7*C*). These data are consistent with the above-mentioned FACS results; however, when we treated those cells with HS lyase, the MFIs of 8-val TatP-QDs on HeLa, HOS, and HepG2 were completely reduced to background levels (data not shown).

DISCUSSION

We obtained a surprising result that strong cell binding can only be achieved with a TatP valence of ≥8 (Fig. 2), and monovalent TatP has a negligible binding capacity (Fig. 1). Although it has been proposed that electrostatic interactions mediate TatP cell binding (9, 14–16), the electric charge of St-QD cannot account for the negligible binding capacity of monovalent

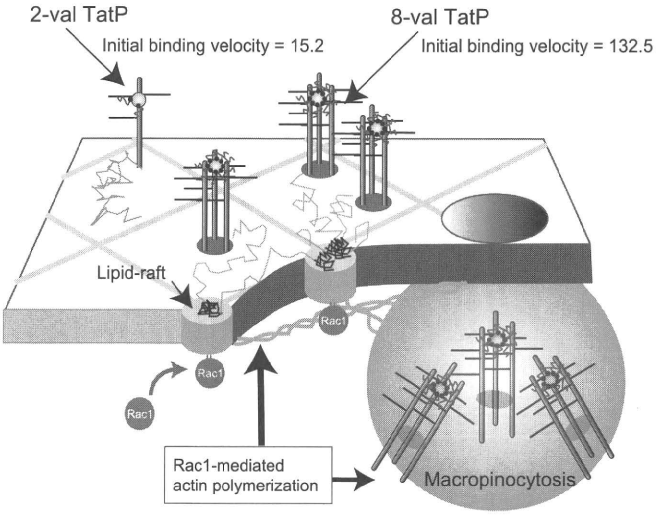

FIGURE 8. **A model showing the events in plasma membrane exposed to 2-val and 8-val TatP.** HSPG exists as a monomer; 8-val TatP clusters with several HSPGs, leading to recruitment of Rac1 to lipid rafts, which triggers membrane reorganization of actin filaments and/or actin-dependent domains and induces the temporary immobilization and clustering of 8-val TatP/HSPGs. Rac1 activation induces TatP/HSPG internalization through macropinocytosis.

TatP-QD. The net charge Z_p is approximately −18, as each QD contains ~30 Sts, and the Z_p of each St is −0.6. This charge could be offset by two biotin-TatPs (total Z_p = 15.8). The very weak binding by monovalent TatP was also measured with two other techniques (FITC-TatP and St-Alexa488 (total Z_p = −2.4) labeled TatP) (Fig. 1*C*). Multivalent TatP (experiments with both St-Alexa488 and -QD) showed a significant amount of binding after 15 min of exposure (Figs. 1*C* and 2). The very weak surface binding is intrinsic to TatP rather than the labeling method. It is common in biological systems that the strength of a ligand-receptor pair is enhanced with multivalency. The chemical and physical mechanisms underlying this phenomenon are not well understood, however, mainly due to the lack of effective assays to detect the strength of cell-surface binding in living cells. Here, we show that single molecule microscopy with particles resistant to photobleaching can be employed as a tool to measure binding in living cells.

We also found that the cell-surface HS chains of HSPG, and not the lipid phosphate groups, are essential for TatP binding, as demonstrated with the enzymatic removal of HS (Fig. 5) and simultaneous observation of two individual molecules (Fig. 6). This result is consistent with a previous report (35) demonstrating that TatP can bind to HS/heparin in the liquid phase with a dissociation constant that is ~2–3 orders of magnitude smaller than in the absence of lipid phosphate groups (48).

Both the trajectory and the *mD* of 2-val TatP, which is unlikely to induce HSPG cross-linking, were found to be similar to that of CD4 (Fig. 3). Thus, the species of HSPG that binds to TatP might initially exist as a monomer (Fig. 8). When 8-val TatP cross-links with the HSPG, Rac1 is activated, inducing frequent, constitutive recruitment of 8-val TatP/TatRs to actin-associated lipid raft microdomains. The 8-val TatP/TatRs that are recruited to these domains have reduced degrees of freedom, probably through Rac1-mediated membrane actin polymerization. Thus, 8-val TatP lipid raft association is more likely to occur. Accordingly, we observed that ≥2 of each 8-val TatP-TatR complex is located in close proximity to a confined area of the plasma membrane that is below the resolution of the microscope. We found that 8-val TatP exposure activates membrane ruffling and increases the level of macropinocytosis through Rac1-dependent mechanisms (Fig. 4, *B–D*). Notably, cell-bound 8-val TatP could be internalized when as few as ~30 8-val particles/cell were attached. In contrast, when ~400 2-val TatP particles/cell were attached, only marginal internalization occurred by 1 h after exposure (data not shown). We found that the initial cell-surface binding velocity of 8-val TatP is only ~6-fold higher than that of 2-val TatP (Fig. 2, *C* and *F*), but the number of TatPs entering cells after 1 h is 120-fold higher.[3] By FACS analysis (supplemental Fig. S7), we found that in the presence of heparin both the binding to the surface and the internalization of the 8-val TatPs are completely abrogated. We found that 2-val TatP can bind to the surface, but it remains on the surface for ~1 h. Its binding is also completely abrogated by heparin exposure. Monovalent TatP-QDs could neither bind to the cell surface nor be internalized. Collectively, these results suggest that both the initial binding of cell surface HSPG and the activation of the signal for internalization are essential for the TatP-QDs getting inside the cells. With our recently developed three-dimensional single particle tracking system (22, 30), we observed that after ~35 min of exposure, 8-val TatP completely stops moving randomly and starts to internalize and move toward the nucleus. We also found that 2-val TatP exhibits only random movements near the glass surface.[4] In our system, without binding to the cell surface, no direct translocation on the membrane can be achieved by monovalent TatP-QDs. Thus, we strongly believe that macropinocytosis of TatP/HSPGs is the only route of entry for TatP. Collectively, multivalent TatP induces HSPG cross-linking to recruit activated Rac1 to lipid rafts; it thereby enhances the recruitment of TatP/HSPG to actin-associated microdomains and internalization by macropinocytosis. These results should guide the design of TatP-based peptides with sufficient transduction efficiencies to be used as therapeutic nanocarriers.

Regarding the expression of HSPG in the HeLa, HepG2, and HOS cell lines, we found that the MFIs of F58-10E4 mAb were the highest in HepG2 and the lowest in HeLa cells (Fig. 7*A*). In contrast, the level of 8-val TatP binding to the cellular surface was highest in HOS and lowest in HepG2 (Fig. 7, *B* and *C*). These results suggest that the level of TatP binding in different cell types does not correlate with the levels of F58-10E4 bound to the cells. However, the ability of TatP to bind these cells requires cell-surface GAG chain expression, as the binding capacity of 8-val TatP to the cell surface is totally abrogated by HS lyase treatment. An enormous number of potential GAG structures can be synthesized as part of the complex process of GAG chain synthesis and modification. Specific modified forms of GAG induce the lock-and-key interaction between HS/heparin and ligands and occur in a tissue- and cell type-specific manner (45). We hypothesize that TatP-specific GAG units are preferentially added in some cell types or some types

[3] J. Imamura, unpublished results.
[4] Y. Suzuki, unpublished results.

of HSPGs. Consequently, the level of TatP bound to the cell could vary regardless of the level of F58-10E4 bound to those cells. It has also been shown that HSPG always works as a co-receptor with various other factors. Thus, another possible explanation is that TatP binds to an unidentified secondary cell-surface receptor, which determines the level of TatP binding to the cell surface. As subfamilies of HSPGs exist (45), future studies should focus on the identification of the relevant HSPGs, the structural determinants within the HS chains that mediate TatP binding, and the secondary TatRs.

We have not confirmed that our findings are applicable *in vivo*; however, we have already reported that our visualization system can track a single tumor-targeting antibody-QD in tumors of live mice (49). Therefore, future studies can focus on whether multivalent TatP-QDs can efficiently bind to and be taken up by cells *in vivo*.

Acknowledgment—We thank Dr. Toshio Hattori for logistical support in performing the study.

REFERENCES

1. Frankel, A. D., and Pabo, C. O. (1988) *Cell* **55,** 1189–1193
2. Green, M., and Loewenstein, P. M. (1988) *Cell* **55,** 1179–1188
3. Chauhan, A., Tikoo, A., Kapur, A. K., and Singh, M. (2007) *J. Control Release* **117,** 148–162
4. Fawell, S., Seery, J., Daikh, Y., Moore, C., Chen, L. L., Pepinsky, B., and Barsoum, J. (1994) *Proc. Natl. Acad. Sci. U.S.A.* **91,** 664–668
5. Vivès, E., Brodin, P., and Lebleu, B. (1997) *J. Biol. Chem.* **272,** 16010–16017
6. Nagahara, H., Vocero-Akbani, A. M., Snyder, E. L., Ho, A., Latham, D. G., Lissy, N. A., Becker-Hapak, M., Ezhevsky, S. A., and Dowdy, S. F. (1998) *Nat. Med.* **4,** 1449–1452
7. Sodroski, J., Patarca, R., Rosen, C., Wong-Staal, F., and Haseltine, W. (1985) *Science* **229,** 74–77
8. Schwarze, S. R., Ho, A., Vocero-Akbani, A., and Dowdy, S. F. (1999) *Science* **285,** 1569–1572
9. Wadia, J. S., Stan, R. V., and Dowdy, S. F. (2004) *Nat. Med.* **10,** 310–315
10. Sandgren, S., Cheng, F., and Belting, M. (2002) *J. Biol. Chem.* **277,** 38877–38883
11. Rusnati, M., Coltrini, D., Oreste, P., Zoppetti, G., Albini, A., Noonan, D., d'Adda, di Fagagna, F., Giacca, M., and Presta, M. (1997) *J. Biol. Chem.* **272,** 11313–11320
12. Tyagi, M., Rusnati, M., Presta, M., and Giacca, M. (2001) *J. Biol. Chem.* **276,** 3254–3261
13. Gump, J. M., June, R. K., and Dowdy, S. F. (2010) *J. Biol. Chem.* **285,** 1500–1507
14. Dathe, M., Schümann, M., Wieprecht, T., Winkler, A., Beyermann, M., Krause, E., Matsuzaki, K., Murase, O., and Bienert, M. (1996) *Biochemistry* **35,** 12612–12622
15. Mishra, A., Gordon, V. D., Yang, L., Coridan, R., and Wong, G. C. (2008) *Angew. Chem. Int. Ed. Engl.* **47,** 2986–2989
16. Suzuki, T., Futaki, S., Niwa, M., Tanaka, S., Ueda, K., and Sugiura, Y. (2002) *J. Biol. Chem.* **277,** 2437–2443
17. Xiao, H., Neuveut, C., Tiffany, H. L., Benkirane, M., Rich, E. A., Murphy, P. M., and Jeang, K. T. (2000) *Proc. Natl. Acad. Sci. U.S.A.* **97,** 11466–11471
18. Barillari, G., Gendelman, R., Gallo, R. C., and Ensoli, B. (1993) *Proc. Natl. Acad. Sci. U.S.A.* **90,** 7941–7945
19. Toschi, E., Bacigalupo, I., Strippoli, R., Chiozzini, C., Cereseto, A., Falchi, M., Nappi, F., Sgadari, C., Barillari, G., Mainiero, F., and Ensoli, B. (2006) *Mol. Biol. Cell* **17,** 1985–1994
20. Albini, A., Soldi, R., Giunciuglio, D., Giraudo, E., Benelli, R., Primo, L., Noonan, D., Salio, M., Camussi, G., Rockl, W., and Bussolino, F. (1996) *Nat. Med.* **2,** 1371–1375
21. Liu, Y., Jones, M., Hingtgen, C. M., Bu, G., Laribee, N., Tanzi, R. E., Moir, R. D., Nath, A., and He, J. J. (2000) *Nat. Med.* **6,** 1380–1387
22. Watanabe, T. M., Sato, T., Gonda, K., and Higuchi, H. (2007) *Biochem. Biophys. Res. Commun.* **359,** 1–7
23. Nguyen, V. T., Kamio, Y., and Higuchi, H. (2003) *EMBO J.* **22,** 4968–4979
24. Medintz, I. L., Uyeda, H. T., Goldman, E. R., and Mattoussi, H. (2005) *Nat. Mater.* **4,** 435–446
25. Jaiswal, J. K., Mattoussi, H., Mauro, J. M., and Simon, S. M. (2003) *Nat. Biotechnol.* **21,** 47–51
26. David, G., Bai, X. M., Van der Schueren, B., Cassiman, J. J., and Van den Berghe, H. (1992) *J. Cell Biol.* **119,** 961–975
27. Gómez-Moutón, C., Lacalle, R. A., Mira, E., Jiménez-Baranda, S., Barber, D. F., Carrera, A. C., Martínez-A, C., and Mañes, S. (2004) *J. Cell Biol.* **164,** 759–768
28. Suzuki, Y., Rahman, M., and Mitsuya, H. (2001) *J. Immunol.* **167,** 3064–3073
29. Suzuki, K. G., Fujiwara, T. K., Sanematsu, F., Iino, R., Edidin, M., and Kusumi, A. (2007) *J. Cell Biol.* **177,** 717–730
30. Watanabe, T. M., and Higuchi, H. (2007) *Biophys. J.* **92,** 4109–4120
31. Gonda, K., Watanabe, T. M., Ohuchi, N., and Higuchi, H. (2010) *J. Biol. Chem.* **285,** 2750–2757
32. Hikage, M., Gonda, K., Takeda, M., Kamei, T., Kobayashi, M., Kumasaka, M., Watanabe, M., Satomi, S., and Ohuchi, N. (2010) *Nanotechnology* **21,** 185103
33. Ruan, G., Agrawal, A., Marcus, A. I., and Nie, S. (2007) *J. Am. Chem. Soc.* **129,** 14759–14766
34. Lidke, D. S., Lidke, K. A., Rieger, B., Jovin, T. M., and Arndt-Jovin, D. J. (2005) *J. Cell Biol.* **170,** 619–626
35. Ziegler, A., and Seelig, J. (2004) *Biophys. J.* **86,** 254–263
36. Kusumi, A., Nakada, C., Ritchie, K., Murase, K., Suzuki, K., Murakoshi, H., Kasai, R. S., Kondo, J., and Fujiwara, T. (2005) *Annu. Rev. Biophys. Biomol. Struct.* **34,** 351–378
37. Fujiwara, T., Ritchie, K., Murakoshi, H., Jacobson, K., and Kusumi, A. (2002) *J. Cell Biol.* **157,** 1071–1081
38. Hall, A. (2005) *Biochem. Soc. Trans.* **33,** 891–895
39. Grimmer, S., van Deurs, B., and Sandvig, K. (2002) *J. Cell Sci.* **115,** 2953–2962
40. del Pozo, M. A., Alderson, N. B., Kiosses, W. B., Chiang, H. H., Anderson, R. G., and Schwartz, M. A. (2004) *Science* **303,** 839–842
41. Grande-García, A., Echarri, A., and Del Pozo, M. A. (2005) *Biochem. Soc. Trans.* **33,** 609–613
42. Ridley, A. J., Paterson, H. F., Johnston, C. L., Diekmann, D., and Hall, A. (1992) *Cell* **70,** 401–410
43. Kaplan, I. M., Wadia, J. S., and Dowdy, S. F. (2005) *J. Control. Release* **102,** 247–253
44. Mayor, S., and Pagano, R. E. (2007) *Nat. Rev. Mol. Cell Biol.* **8,** 603–612
45. Esko, J. D., and Lindahl, U. (2001) *J. Clin. Invest.* **108,** 169–173
46. Bartholomew, J. S., Handley, C. J., and Lowther, D. A. (1985) *Biochem. J.* **227,** 429–437
47. Piñon, J. D., Klasse, P. J., Jassal, S. R., Welson, S., Weber, J., Brighty, D. W., and Sattentau, Q. J. (2003) *J. Virol.* **77,** 9922–9930
48. Ziegler, A., Blatter, X. L., Seelig, A., and Seelig, J. (2003) *Biochemistry* **42,** 9185–9194
49. Tada, H., Higuchi, H., Wanatabe, T. M., and Ohuchi, N. (2007) *Cancer Res.* **67,** 1138–1144

厚生労働科学研究費補助金エイズ対策研究事業
「抗HIV薬の適正使用と効果・毒性に関する基礎的研究」班
平成22年度　総括・分担研究報告書

発行日　2011年3月31日

発行者　研究代表者　潟永　博之

発行所　研究班事務局
（独）国立国際医療研究センターエイズ治療・研究開発センター
〒162-8655　東京都新宿区戸山1-21-1